Electronic Supplementary Information (ESI)

Unexpected structural transformation into noria-like Ag_{13} metal cluster and copper-doping induced boost in photoluminescence

Su-Kao Peng,[a†] Zhou Lu,[a†§] Mo Xie,[a] Yong-Liang Huang,[a] Dong Luo,[a] Jia-Nan Wang,[a] Xiao-Wei Zhu,[a] Xue Li,[b] Xiao-Ping Zhou,*[a] and Dan Li*[a]

[a.] College of Chemistry and Materials Science, Jinan University, Guangzhou 510632, P. R. China. E-mail: zhouxp@jnu.edu.cn, danli@jnu.edu.cn

[b.] Institute of Mass Spectrometry and Atmospheric Environment, Jinan University, Guangzhou 510632, P. R. China.

† S.-K.P. and Z.L. contributed equally to this work.

§ Present address: Department of Chemistry, University of North Texas, Denton, Texas 76203, United States.

Physical measurement and instrumentation

All starting materials were purchased from commercial sources and used as received without further purification. The solvents used for synthesis were of analytical grade. Fourier-transfer infrared (FT-IR) spectra were recorded on a Thermo Scientific FT-IR Nicolet iS10 spectrophotometer in the frequency range from 4000 – 400 cm^{-1}. The solid-state ultraviolet-visible (UV-vis) absorption spectra were recorded on a Bio-Logic MOS-500 multifunctional circular dichroism spectrometer; while solution UV-vis absorption spectra were conducted by Agilent Cary 4000 UV-Vis spectrophotometer. Elemental analyses were determined by Elementar vario Micro Cube. Powder X-ray diffraction (PXRD) experiments were performed on a Rigaku Ultima IV X-ray diffractometer (Cu Kα, λ=1.5418 Å) in the step of 0.02˚ under the tube conditions 40 KV and 40 mA. The thermogravimetry analyses (TGA) were carried out on TGA Q50 V20.6 with a heating rate of 10 ˚C/min from 30 to 800 ˚C in N_2 atmosphere. The NMR signals were recorded by Bruker Ascend 400, using CD_3CN as solvent. Inductively coupled plasma-atomic emission spectroscopy (ICP-AES) was performed on Thermo Scientific iCAP 7000 series ICP-OES instrument; X-ray photoelectron spectroscopy (XPS) was finished by Thermo Fisher 250XI model. Energy dispersive X-ray spectroscopy (EDX) was carried out by Bruker X-Flash 6130 model. Mass spectra were obtained from a Hexin atmospheric pressure interface-time-of-flight mass spectrometer (API-TOFMS II) in using electrospray ionization (ESI) and a Thermo Scientific Q Exactive hybrid quadrupole-orbitrap mass spectrometer or a Hexin matrix-assisted laser desorption ionization time-of-flight mass spectrometer (MALDI-TOF-MS) adopting 2,5-dihydroxybenzoic acid (DHB) as matrix. All mass spectrometric analyses were done in HPLC-grade acetonitrile or methanol solution.

Steady-state photoluminescence spectra for all sample were recorded on a Horiba FluoroMax-4 fluorometer and Janis VPF-100 cryostat system was used for temperature-controlled measurement by adopting liquid nitrogen. Decay curves were recorded on an Edinburgh FLS920 spectrometer equipped with a μF900 μs flash lamp and a closed cycle cryostat (Advanced Research Systems) with liquid helium as cooling media. The absolute photoluminescence quantum yields were measured by employing Hamamatsu C11347-01 absolute PL quantum yield spectrometer under both room temperature and liquid nitrogen. In solid sample state, crystalline samples were used for all photoluminescence measurements. The crystalline phase purity of the samples was assured by elemental analyses and powder X-ray diffraction measurements.

Single crystals data collections were performed on an Oxford Diffraction XtalAB [Rigaku(Cu) X-ray dual wavelength source, Kα, λ =1.5418 Å] equipped with a monochromator and CCD plate detector (CrysAlisPro CCD, Oxford Diffraction Ltd) at 100 K. Structures were solved by using direct methods by ShelXT[1] in OLEX2 program package[2], and all non-hydrogen atoms were refined with anisotropically by the full-matrix least-square method on F^2 by using the ShelXL program[3]. The hydrogen atoms were located from different maps and refined with isotropic temperature factors. The treatment for the disordered guest molecules and triethylammonium in the cavities involves the use of the SQUEEZE program of PLATON. In $\mathbf{Ag_{11.8}Cu_{1.2}}$ and $\mathbf{Ag_{11.3}Cu_{1.7}}$ structures, Ag and Cu atoms exhibited positional disorder. Detailed structure refinement information was appended in the CIF files. Crystal data and structure refinement parameters are summarized in Table S1. Selected bond lengths and angles are given in Table S7 – S9. CCDC nos. 1899535-1899537. These data can be obtained free of charge from The Cambridge Crystallographic Data Centre.

Experimental Procedures

$[Ag(3,5\text{-}(CF_3)_2\text{-}pz)]_3$ (**Ag_3pz_3**) and $[Cu(3,5\text{-}(CF_3)_2\text{-}pz)]_3$ (**Cu_3pz_3**) were synthesized following the literature methods.[4]

Synthesis of **Ag_{13}**:
To 1 mL benzene solution of 0.01 mL phenylacetylene, **Ag_3pz_3** (15.0 mg, 0.016 mmol) was added to afford clear yellowish solution. Et_3N/*n*-hexane (1:100, v:v) vapours were allowed to slowly diffuse into the solution in a sealed vial for overnight in dark to obtain colourless crystals of **Ag_{13}** (yield: 10.7 mg, 81.8% based on **Ag_3pz_3**). FT-IR (KBr pellet): 2036 cm^{-1} (w, C≡C). ^{1}H NMR (400 MHz, [D3]CD_3CN): δ = 1.18 (t, 9.0, -CH_3 of triethyl amine); 2.99 (q, 6.0, -CH_2 of triethyl amine); 6.57 (s, 6.0, -pyrazolate); 7.12-7.24 (m, 29.0, -phenylacetylide). Elemental analysis for $C_{94}H_{46}Ag_{13}F_{36}N_{12}{\cdot}C_6H_{16}N$, calcd (%): C 34.01, H 1.77, N 5.16; found: C 33.89, H 2.065, N 5.21.

Synthesis of **$Ag_{11.8}Cu_{1.2}$**:
Procedures identical to that applied for **Ag_{13}** were followed, while using **Ag_3pz_3** (15.0 mg, 0.016 mmol) and **Cu_3pz_3** (3.2 mg, 0.004mmol) for the product **$Ag_{11.8}Cu_{1.2}$** (yield: 11.1 mg, 78.3% based on **Ag_3pz_3**). FT-IR (KBr pellet): 2035 cm^{-1} (w, C≡C). ^{1}H NMR (400 MHz, [D3]CD_3CN): δ = 1.15 (t, 9.0, -CH_3 of triethyl amine); 2.93 (q, 6.0, -CH_2 of triethyl amine); 6.57 (s, 6.1, -pyrazolate); 7.11-7.23 (m, 30.8, -phenylacetylide). Elemental analysis for $C_{94}H_{46}Ag_{11.8}Cu_{1.2}F_{36}N_{12}{\cdot}C_6H_{16}N$, calcd (%): C 34.52, H 1.79, N 5.23; found: C 34.55, H 2.11, N 5.36.

Synthesis of **$Ag_{11.3}Cu_{1.7}$**:
Procedures identical to that applied for **Ag_{13}** were followed, while using **Ag_3pz_3** (15.0 mg, 0.016 mmol) and **Cu_3pz_3** (5.1 mg, 0.0064mmol) for the product **$Ag_{11.3}Cu_{1.7}$** (yield: 11.8 mg, 80.1% based on **Ag_3pz_3**). FT-IR (KBr pellet): 2035 cm^{-1} (w, C≡C). ^{1}H NMR (400 MHz, [D3]CD_3CN): δ = 1.13 (t, 9.0, -CH_3 of triethyl amine); 2.88 (q, 6.0, -CH_2 of triethyl amine); 6.56 (s, 6.0, -pyrazolate); 7.11-7.23 (m, 30.1, -phenylacetylide). Elemental analysis for $C_{94}H_{46}Ag_{11.3}Cu_{1.7}F_{36}N_{12}{\cdot}C_6H_{16}N$, calcd (%): C 34.74, H 1.81, N 5.27; found: C 34.89, H 1.98, N 5.37.

Computational details

Density functional theory (DFT) calculations were performed using ORCA 4.1.1[5] under the level of GGA-PBE functional[6]. Geometry optimizations and single point energies were conducted using the Karlsruhe def2-SVP basis set[7] for C, N, F, H, and Cu atoms with build-in effective

core potential (def2-ECP)[8] for Ag atoms. Auxiliary basis sets def2/J[9] was also adopted for Coulomb fitting. The single crystals were taken as the initial guess for geometry optimizations in -1 charge state by omitting counter-cations. Kohn-Sham orbital maps and population analysis were finished by Multiwfn 3.6[10] and visualized by VMD 1.9.3 program[11]. Time-dependent density functional theory (TD-DFT) calculations were conducted by AMS 2018 program package.[12] GGA-PBE functional and triple-zeta polarization (TZP) basis set[13] with small frozen core approximation were employed for all atoms. Treatment of ZORA Hamiltonian was adopted for scalar relativistic effects.[14] For calculation of singlet excited states, first 150 states were considered for analysis of assignments and natural transition orbitals (NTOs). Also, first 1500 singlet excited states were calculated using TD-DFT+TB (tight-binding) formalism,[15] which relied on DFT-based ground state calculations as input to an excited state calculation with TD-density functional tight binding (TD-DFTB) coupling matrices for the linear response, to simulate absorption spectra in an affordable computational cost.

The calculating model of **Ag_{13}** is extracted from single crystal and fully-optimized; models of bimetallic Ag/Cu nanoclusters are constructed from single crystals of **$Ag_{11.8}Cu_{1.2}$** and **$Ag_{11.3}Cu_{1.7}$** and optimized by fixing central (1A or 1B) and noria-position (4B and 4B') copper atoms based on DFT conformation studies, marked as **[$Cu@Ag_{12}$]** and **[$Cu@Ag_{10}Cu_2$]**, respectively.

Results and Discussion

Table S1. Summary of crystal data and structure refinement parameter of **Ag_{13}**, **$Ag_{11.8}Cu_{1.2}$**, and **$Ag_{11.3}Cu_{1.7}$**.

	Ag_{13}	**$Ag_{11.8}Cu_{1.2}$**	**$Ag_{11.3}Cu_{1.7}$**
CCDC no.	1899535	1899536	1899537
Empirical formula	$C_{94}H_{46}Ag_{13}F_{36}N_{12}$	$C_{94}H_{46}Ag_{11.96}CuF_{36}N_{12}$	$C_{94}H_{46}Ag_{11.5}Cu_{1.5}F_{36}N_{12}$
Formula weight	3429.74	3381.09	3363.24
Temperature (K)	100(10)	100(10)	100(10)
Crystal system	Triclinic	Triclinic	Triclinic
space group	*P*-1	*P*-1	*P*-1
a (Å)	15.3728(4)	15.5019(4)	15.4952(4)
b (Å)	15.4794(4)	15.7093(4)	15.5896(3)
c (Å)	15.4872(4)	15.9495(6)	15.5997(3)
α (°)	61.894(3)	60.608(3)	61.283(2)
β (°)	68.689(2)	65.701(3)	67.640(2)
γ (°)	61.905(3)	61.289(3)	61.420(2)
Volume (Å^3)	2819.87(16)	2888.55(19)	2846.14(13)
Z	1	1	1
ρ_{calc} (g/cm^3)	2.020	1.944	1.962
F (000)	1629	1609	1602
Theta range for data collection (°)	[2.340, 31.067]	[5.558, 78.239]	[5.111, 78.223]
Total reflections	112942	30961	33504
Unique reflections	16203	11777	11751
R_{int}	0.0398	0.0332	0.0323
Completeness (%)	99.9	99.3	99.6
Data / restraints / parameters	16203 / 143 / 724	11777 / 359 / 771	11751 / 84 / 673
GOOF	1.013	1.038	1.050
R_1[a] [I>2sigma(I)]	0.0342	0.0876	0.0631
$_wR_2$[b] (all data)	0.0756	0.2533	0.1731
Largest diff. peak and hole (e/Å^3)	2.348, -1.570	3.833, -1.735	2.193, -2.049

[a] $R_1=\Sigma||F_o|-|F_c||/\Sigma|Fo|$. [b] $wR_2 = \{[\Sigma w(F_o^2-F_c^2)^2]/\Sigma[w(F_o^2)^2]\}^{1/2}$; $w = 1/[\sigma^2(F_o^2) + (aP)^2 + bP]$, where $P = [\max(F_o^2,0) + 2Fc^2]/3$ for all data.

Table S2. Comparisons of bond lengths (Å) in **Ag_{13}**, **$Ag_{11.8}Cu_{1.2}$**, and **$Ag_{11.3}Cu_{1.7}$**.

Bond type	**Ag_{13}**	**$Ag_{11.8}Cu_{1.2}$**	**$Ag_{11.3}Cu_{1.7}$**
M_{center} - Ag_{noria}	2.9133(2) - 3.1607(3)	2.8551(7) - 3.2712(3)	2.8162(5) - 3.2113(15)
Ag_{noria} - Ag_{noria}	2.8386(4) - 3.3283(4)	2.8367(13) - 3.3078(11)	2.693(7) - 3.3036(9)
M_{center} – $C_{terminal\ of\ central\ ligands}$	2.038(3)	1.931(11)	1.892(8)
Ag_{noria} – $C_{termianl\ of\ surrounding\ ligands}$	2.067(3) - 2.566(3)	2.068(12) - 2.531(10)	2.014(12) - 2.515(7)
M_{noria} - N_{all}	2.109(3) - 2.281(3)	2.117(9) - 2.295(8)	2.083(7) - 2.294(8)

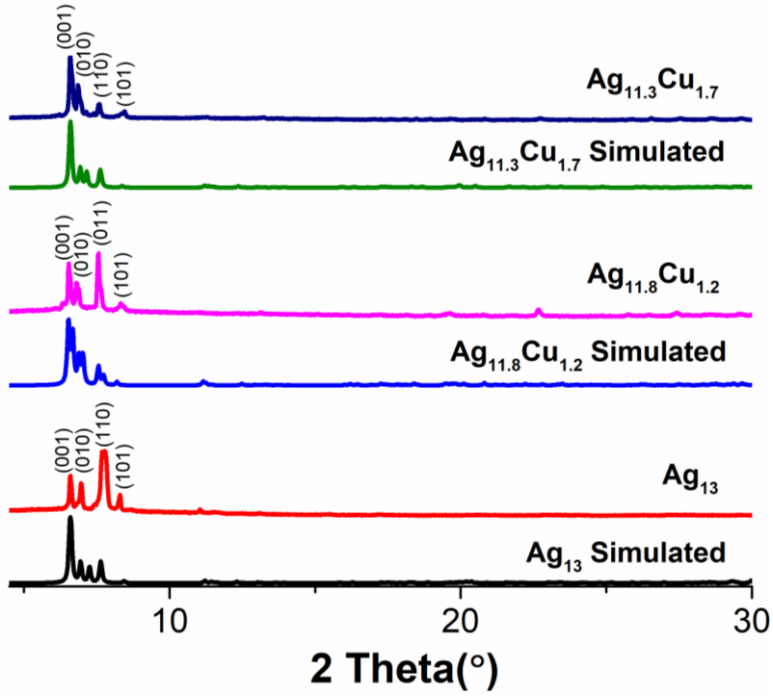

Fig. S1. Powder XRD patterns for simulated and as-synthesized samples of Ag_{13}, $Ag_{11.8}Cu_{1.2}$ and $Ag_{11.3}Cu_{1.7}$.

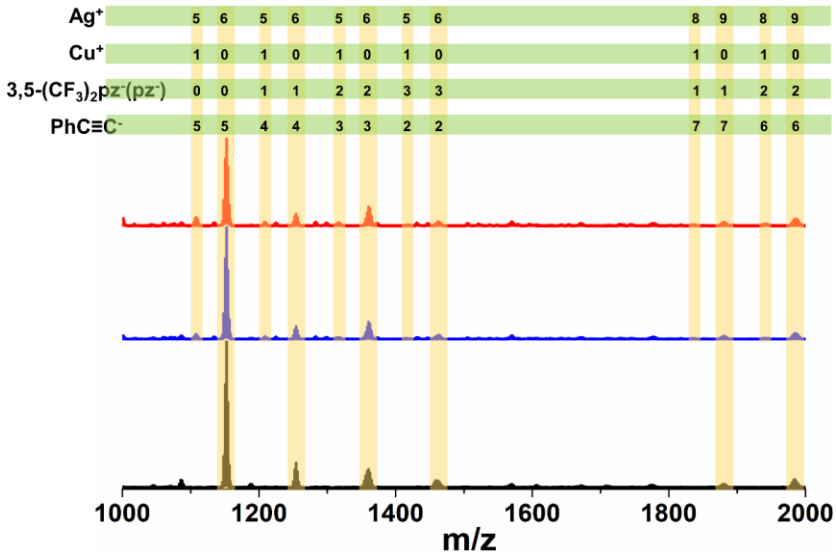

Fig. S2. Mass spectra (m/z range: 1000 – 2000) of (black) Ag_{13}, (blue) $Ag_{11.8}Cu_{1.2}$, (red) $Ag_{11.3}Cu_{1.7}$.

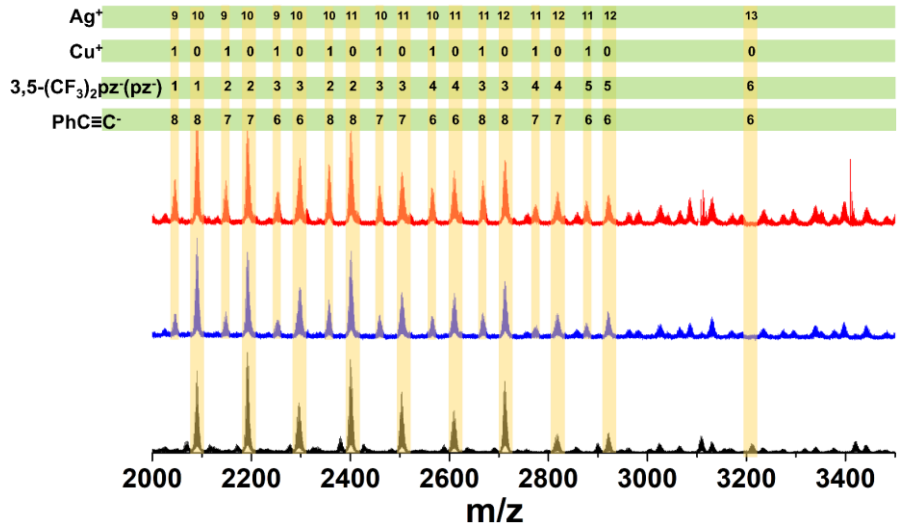

Fig. S3. Mass spectra (m/z range: 2000 – 3000) of (black) Ag_{13}, (blue) $Ag_{11.8}Cu_{1.2}$, (red) $Ag_{11.3}Cu_{1.7}$.

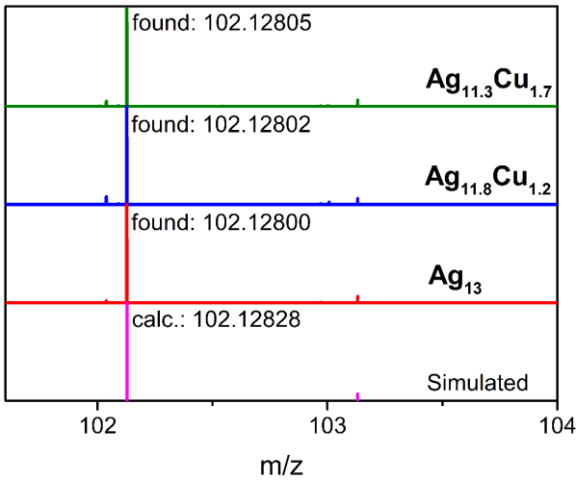

Fig. S4. Mass spectrum of counter cation – triethylammonium (NEt_3H^+) in positive mode.

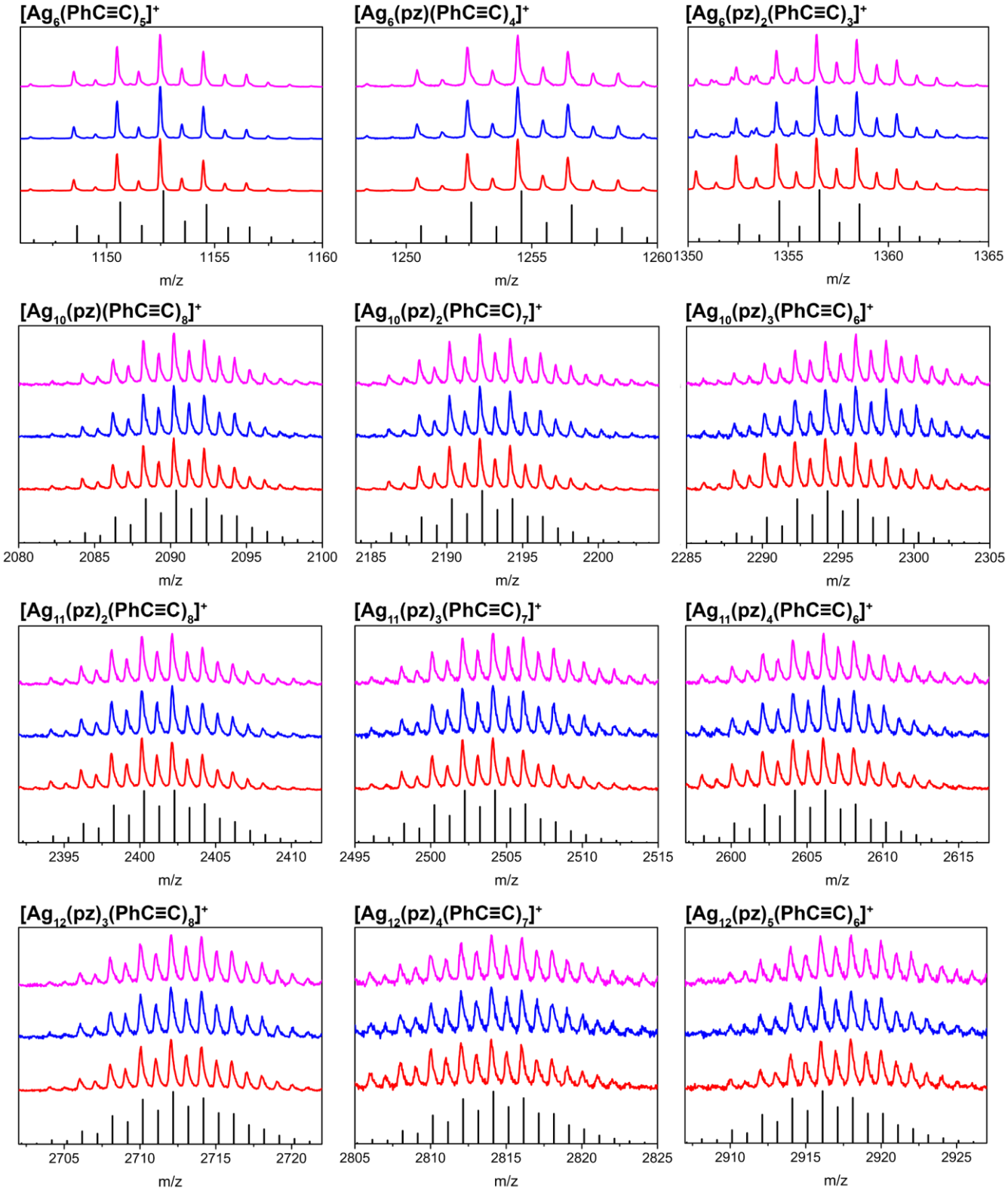

Fig. S5. Mass spectra of all three nanoclusters corresponding to silver-only species. Colour representation: black, simulation; red, Ag_{13}; blue, $Ag_{11.8}Cu_{1.2}$; magenta, $Ag_{11.3}Cu_{1.7}$.

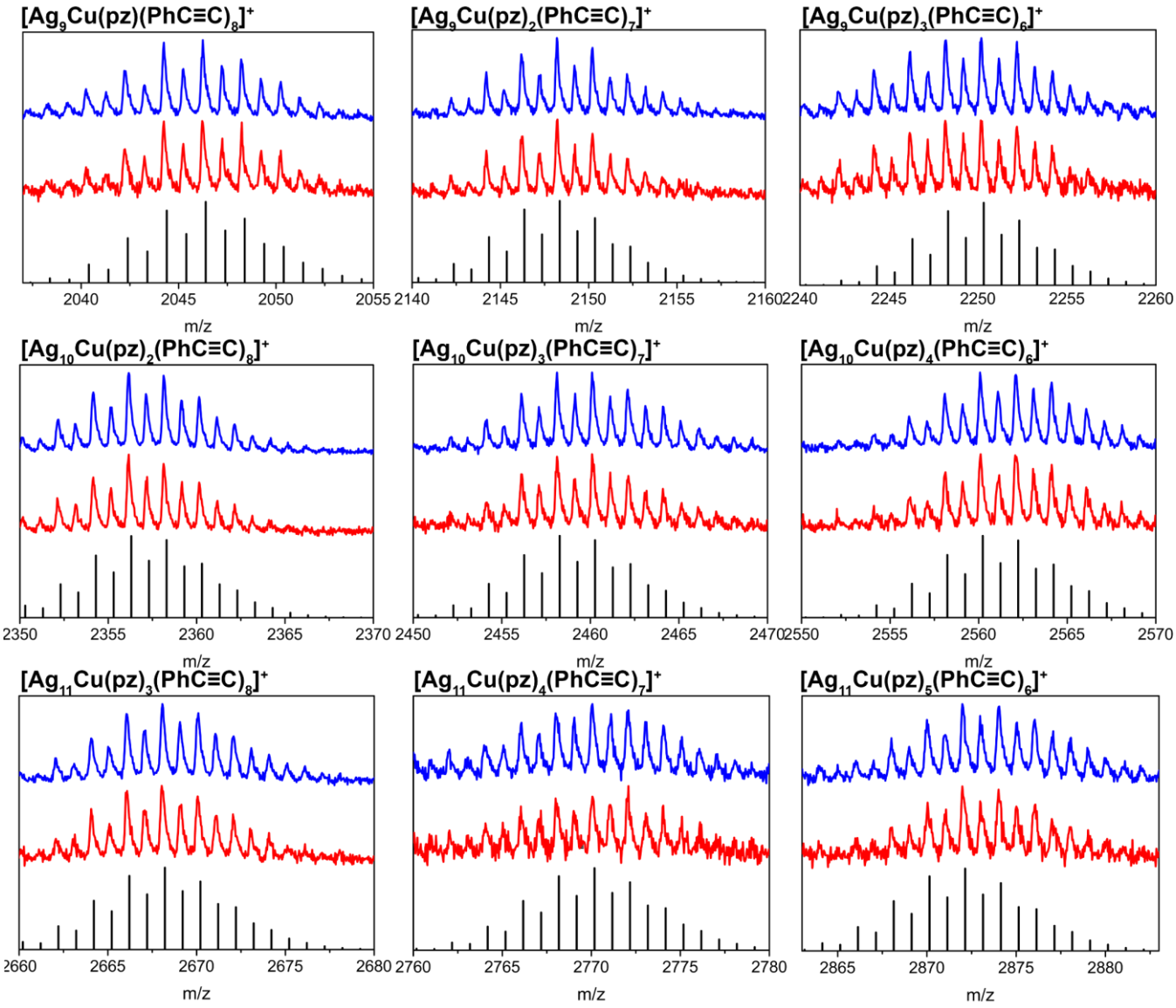

Fig. S6. Mass spectra of bimetallic Ag/Cu nanoclusters corresponding to silver/copper-containing species. Colour representation: black, simulation; red, $Ag_{11.8}Cu_{1.2}$; blue, $Ag_{11.3}Cu_{1.7}$.

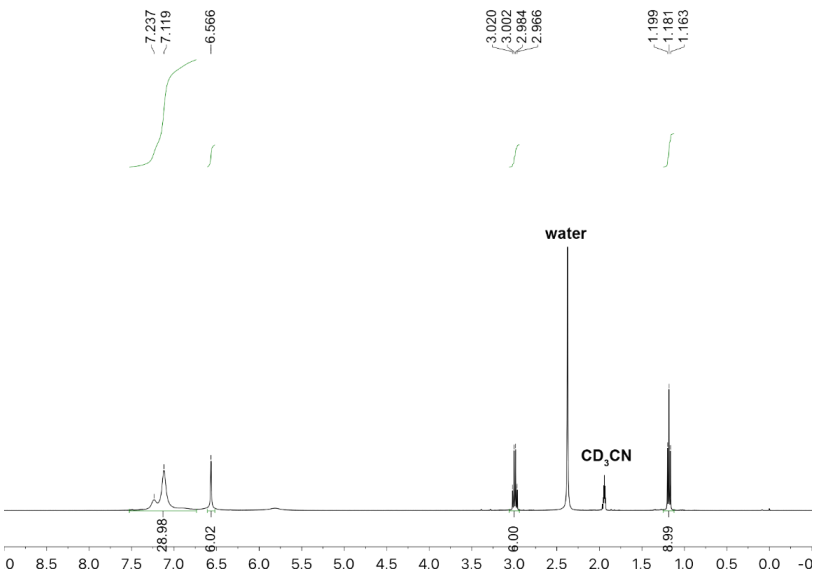

Fig. S7. ^{1}H NMR spectrum of **Ag_{13}** in CD_3CN.

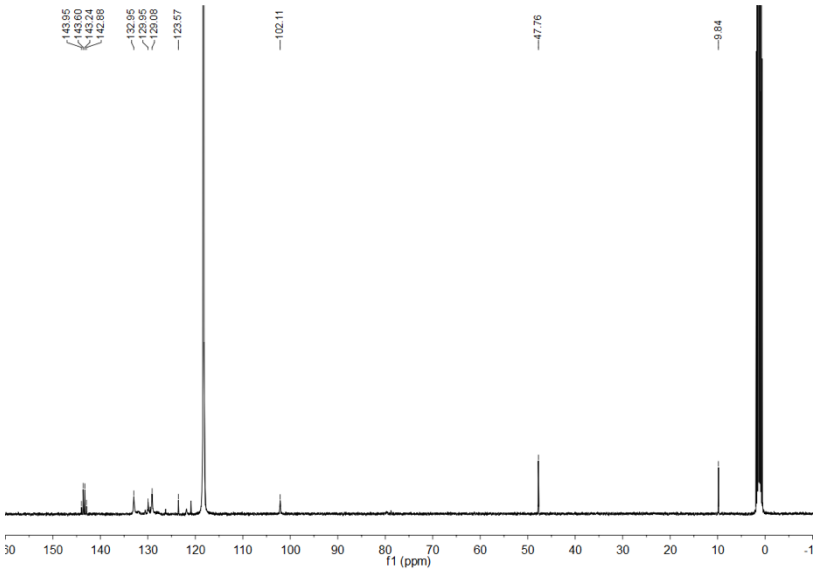

Fig. S8. ^{13}C NMR spectrum of **Ag_{13}** in CD_3CN.

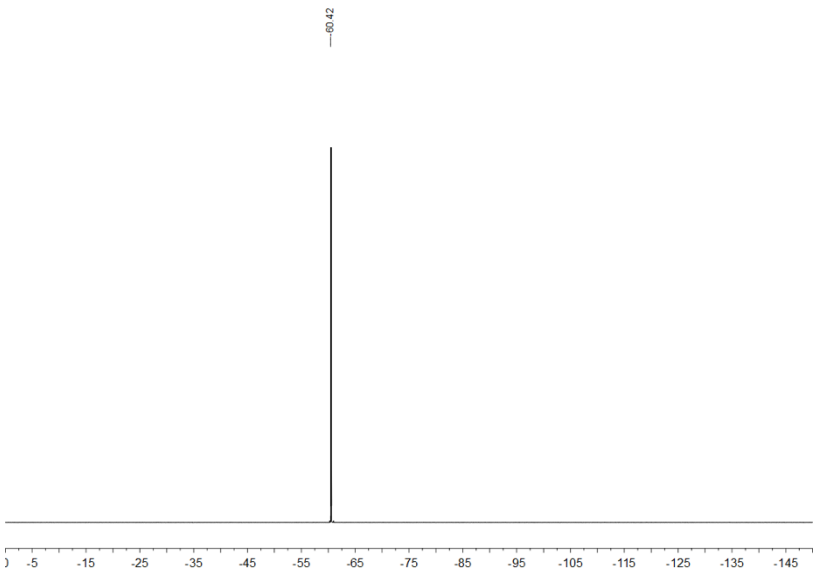

Fig. S9. ^{19}F NMR spectrum of **Ag_{13}** in CD_3CN.

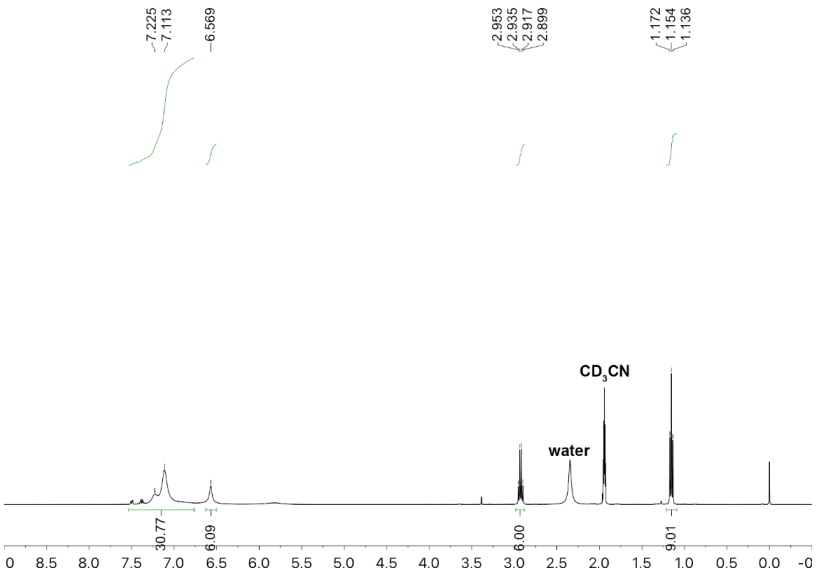

Fig. S10. ^{1}H NMR spectrum of **$Ag_{11.8}Cu_{1.2}$** in CD_3CN.

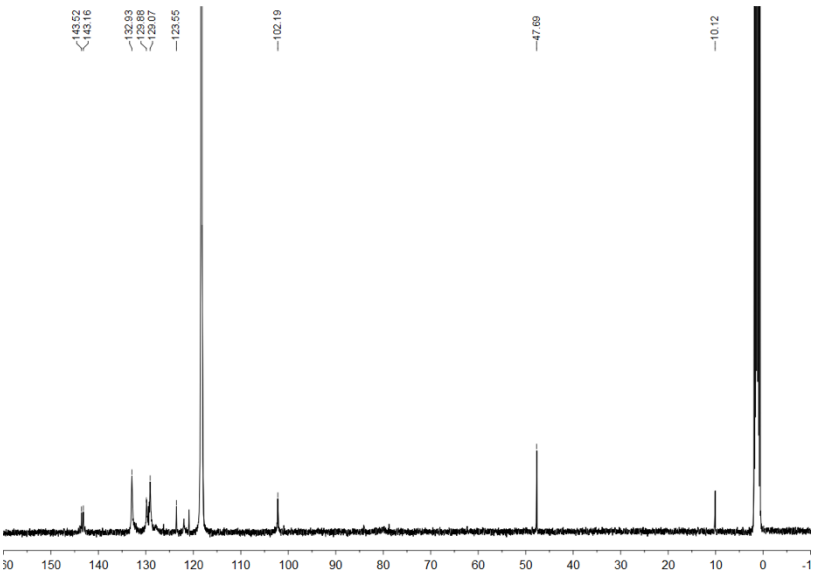

Fig. S11. ^{13}C NMR spectrum of $\mathbf{Ag_{11.8}Cu_{1.2}}$ in CD_3CN.

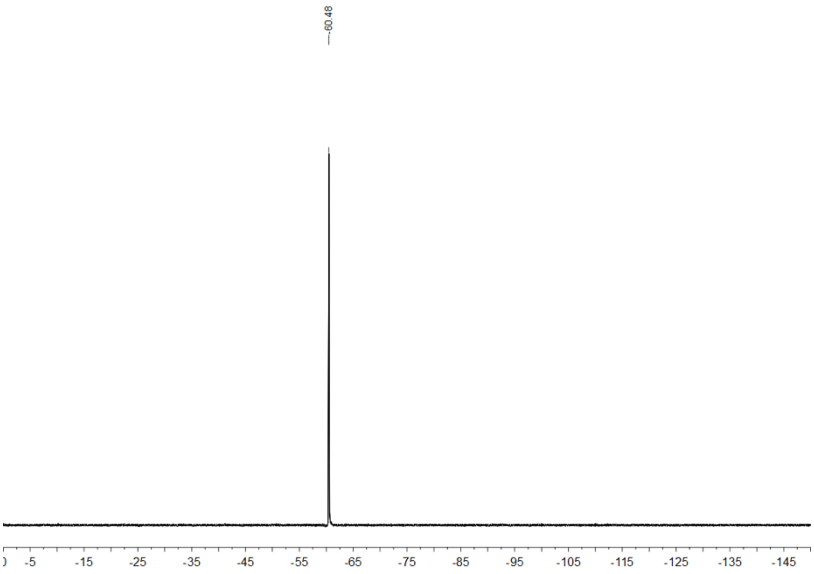

Fig. S12. ^{19}F NMR spectrum of $\mathbf{Ag_{11.8}Cu_{1.2}}$ in CD_3CN.

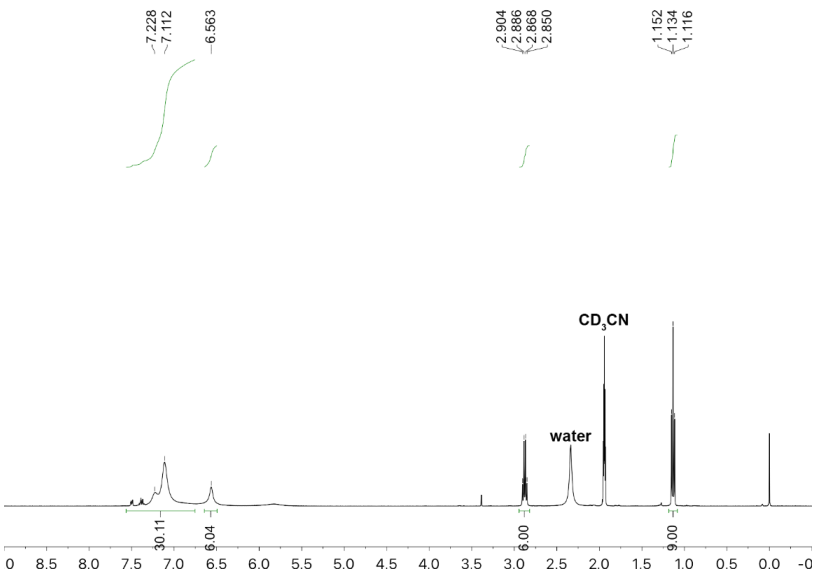

Fig. S13. ^{1}H NMR spectrum of **$Ag_{11.3}Cu_{1.7}$** in CD_3CN.

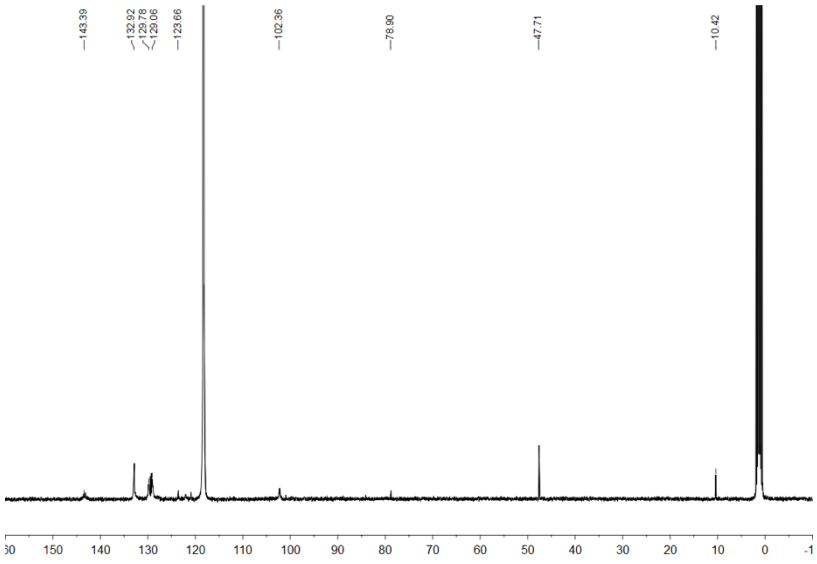

Fig. S14. ^{13}C NMR spectrum of **$Ag_{11.3}Cu_{1.7}$** in CD_3CN.

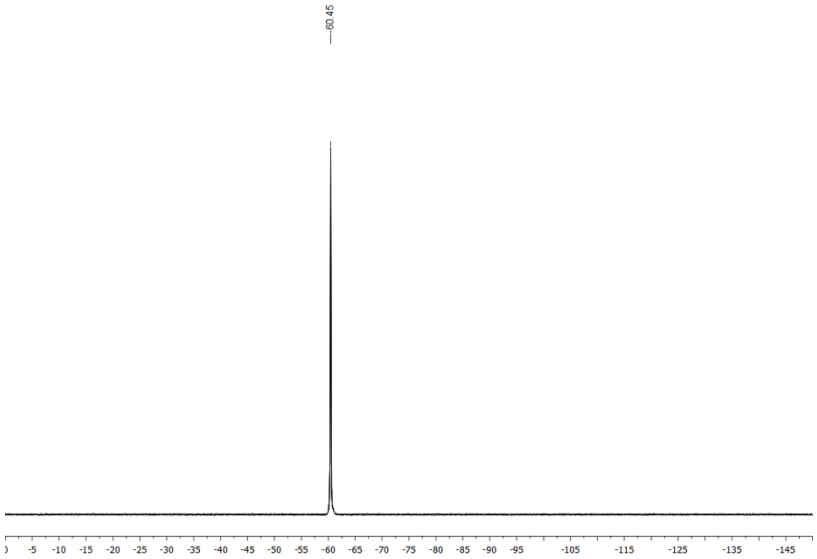

Fig. S15. ^{19}F NMR spectrum of $Ag_{11.3}Cu_{1.7}$ in CD_3CN.

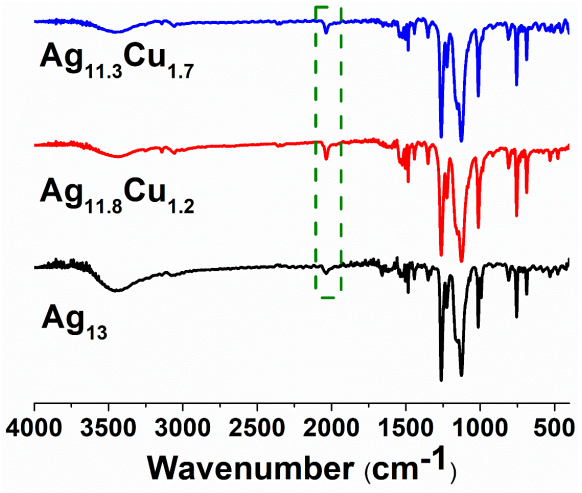

Fig. S16. FT-IR spectra of Ag_{13}, $Ag_{11.8}Cu_{1.2}$, and $Ag_{11.3}Cu_{1.7}$. Circled region indicated stretching vibrations of carbon-carbon triple bonds.

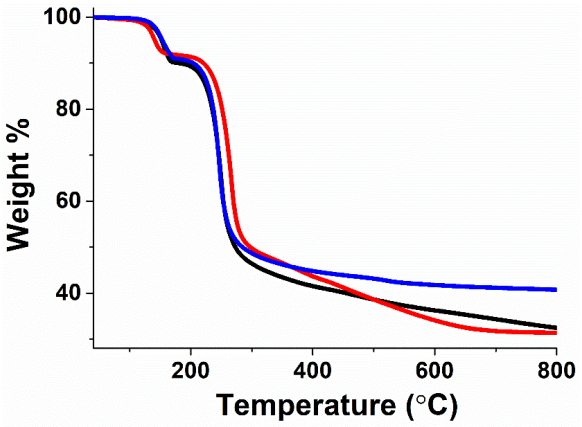

Fig. S17. Thermogravimetric curves of (red) Ag_{13}, (black) $Ag_{11.8}Cu_{1.2}$, and (blue) $Ag_{11.3}Cu_{1.7}$.

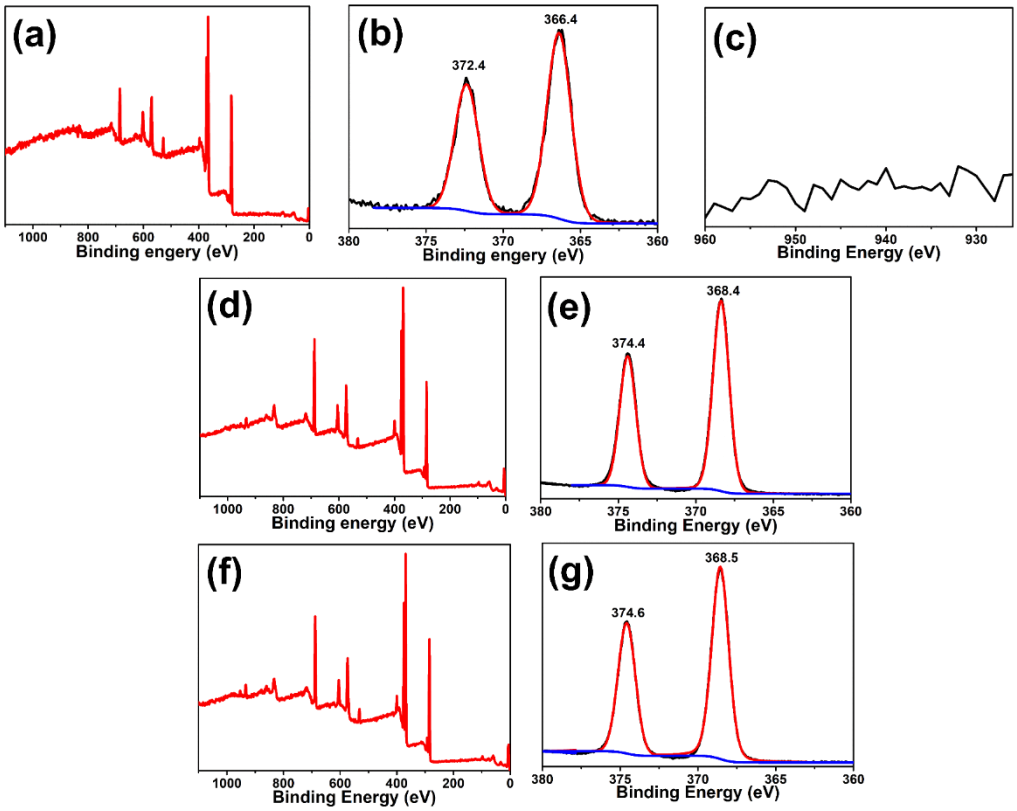

Fig. S18. XPS spectra of (a) Ag_{13}, (d) $Ag_{11.8}Cu_{1.2}$ and (f) $Ag_{11.3}Cu_{1.7}$; XPS binding energies of silver regions for (b) Ag_{13}, (e) $Ag_{11.8}Cu_{1.2}$ and (g) $Ag_{11.3}Cu_{1.7}$; XPS binding energy of copper region for (c) Ag_{13}.

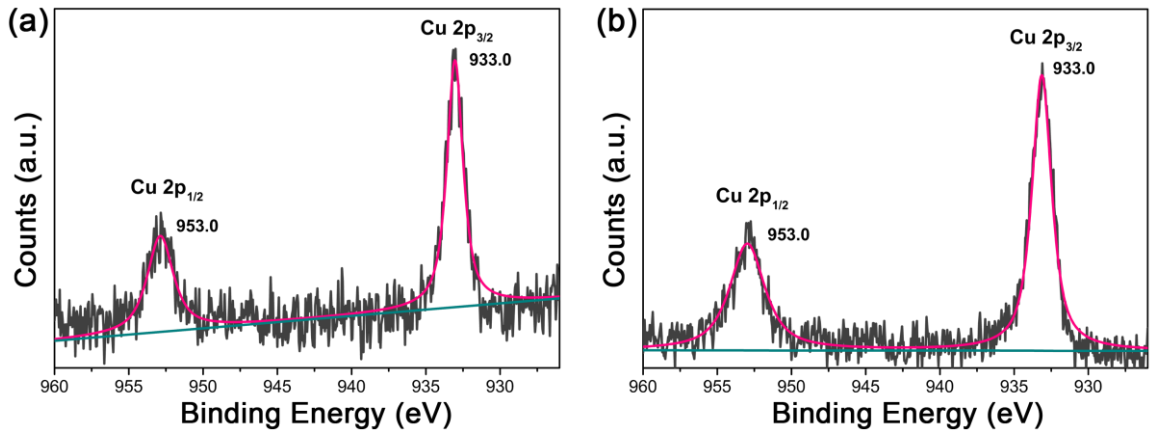

Fig. S19. XPS spectra of (a) $Ag_{11.8}Cu_{1.2}$ and (b) $Ag_{11.3}Cu_{1.7}$ at focused copper region. Fitting curve: solid magenta; fitting baseline: solid green.

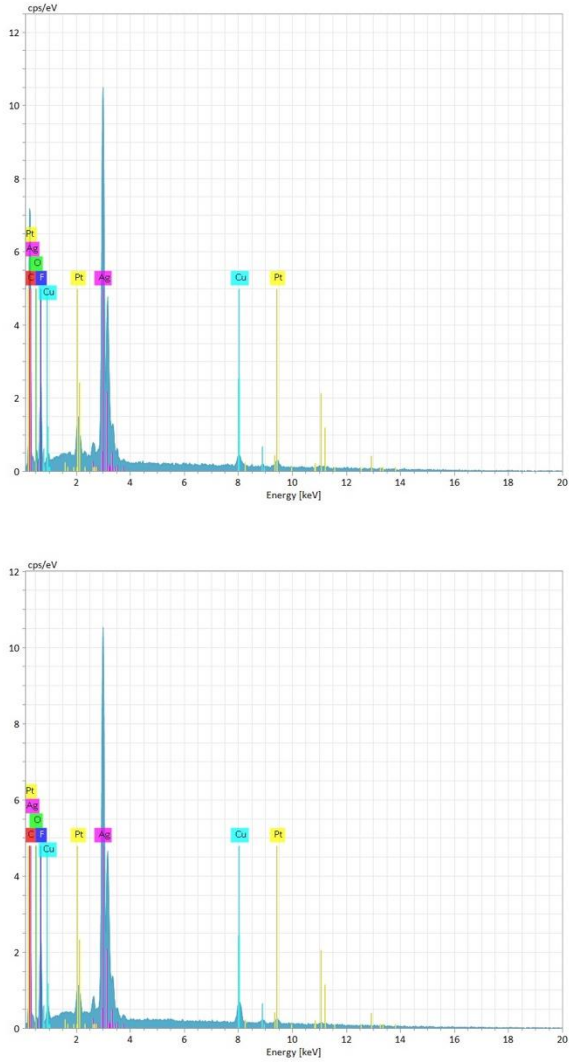

Fig. S20. Energy-dispersive X-ray spectra (EDX) analysis of (top) $Ag_{11.8}Cu_{1.2}$ and (bottom) $Ag_{11.3}Cu_{1.7}$. Elemental content (%) for $Ag_{11.8}Cu_{1.2}$, calcd: Ag 90.77, Cu 9.23; found: Ag 91.91, Cu 8.09; for $Ag_{11.3}Cu_{1.7}$ calcd: Ag 86.92, Cu 13.08; found: Ag 88.66, Cu 11.34.

Table S3. ICP-AES results[a] for $Ag_{11.8}Cu_{1.2}$ and $Ag_{11.3}Cu_{1.7}$.

	ρ(Ag) / ppm	Standard deviation	ρ(Cu) / ppm	Standard deviation	Ag_xCu_{13-x}	
					x	13-x
$Ag_{11.8}Cu_{1.2}$	15.70	0.1185	1.012	0.006871	11.7	1.3
	20.65	0.1387	1.313	0.000437	11.7	1.3
	18.03	0.1378	1.131	0.008207	11.8	1.2
	20.05	0.1865	1.304	0.003469	11.7	1.3
	22.02	0.1576	1.310	0.001953	11.8	1.2
	20.31	0.1723	1.185	0.006042	11.8	1.2
$Ag_{11.3}Cu_{1.7}$	5.678	0.1407	0.5410	0.000453	11.2	1.8
	6.357	0.1375	0.5888	0.006799	11.2	1.8
	6.505	0.2033	0.6068	0.001504	11.3	1.7
	5.872	0.0639	0.5281	0.001246	11.3	1.7
	7.026	0.1207	0.6304	0.006027	11.3	1.7
	5.592	0.0046	0.5222	0.000295	11.2	1.8

[a] All data are from different batches of prepared samples to ensure the reproducibility

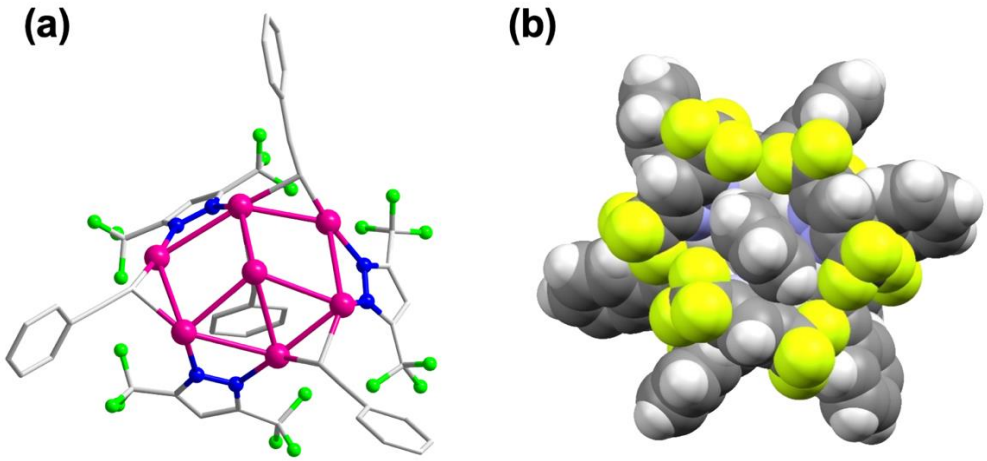

Fig. S21. (a) Asymmetric unit of **Ag_{13}**. (b) Space filling diagram of **Ag_{13}**. Colour representations: magenta, silver; grey, carbon; green, fluorine; blue, nitrogen; white, hydrogen. Disordering phenyl rings are omitted from the figures for clarity.

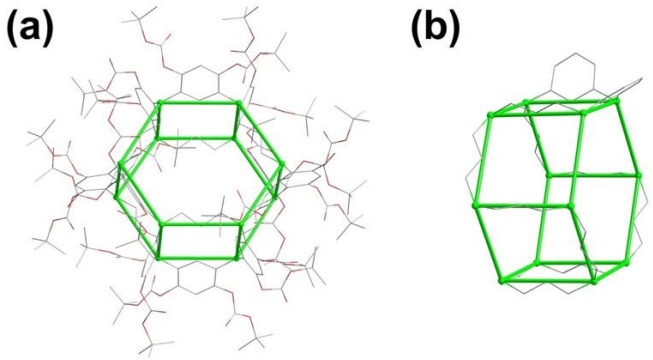

Fig. S22. (a) Crystal structure of noria-BOC from Ref. 16. (b) Simplified structure of noria-BOC showing molecular waterwheel-like skeleton with asymmetric connecting phenyl rings.

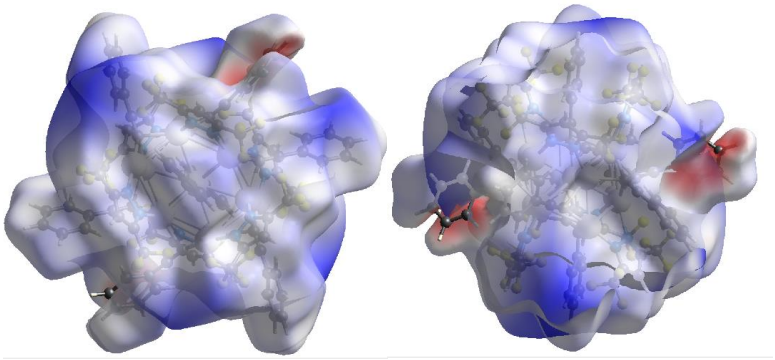

Fig. S23. Hirshfeld surface analysis for **Ag_{13}** (left: top view, right: side view) by Crystal Explorer v17.5[17], showing surface property of d_{norm} (range: -0.02 – 1.00). (Colour red refers potential interacting sites, while white and blue regions represent no inter-cluster interactions. Red regions occur in disordering phenyl ring and mean no potential interacting sites here.)

From the space-filling diagram (Fig. S21b), it also could be noticed that the [Ag_{13}] core is fully protected by bulky phenyl and pz^- moieties besides limited space for disordered counter cationic triethylammonium. No remarkable inter-cluster supramolecular interactions (*e.g.* π-π interaction, hydrogen bonding) could be observed and further confirmed by Hirshfeld surface analysis (Fig. S23).

Table S4. Relative energies (ΔE, kcal/mol), energies of HOMO and LUMO (eV), and HOMO-LUMO gaps($\Delta E_{H\text{-}L}$, eV) of mono- and double-doped copper atoms in different positions at $\mathbf{Ag_{11.8}Cu_{1.2}}$.[a]

1st foreign Cu+ position	2nd foreign Cu+ position	ΔE	E_{HOMO}	E_{LUMO}	$\Delta E_{H\text{-}L}$	1st foreign Cu+ position	2nd foreign Cu+ position	ΔE	E_{HOMO}	E_{LUMO}	$\Delta E_{H\text{-}L}$
1A		0.0	-3.26	-0.80	2.46		2A	2.6	-3.25	-0.80	2.45
2A		17.7	-3.26	-0.81	2.45		3A	2.1	-3.17	-0.82	2.35
3A		16.8	-3.17	-0.83	2.34		4A	0.0	-3.09	-0.80	2.29
4A	N/A[b]	14.8	-3.09	-0.81	2.28	1A	5A	1.0	-3.15	-0.81	2.34
5A		15.5	-3.15	-0.82	2.33		6A	2.9	-3.20	-0.81	2.39
6A		17.9	-3.20	-0.82	2.38		7A	1.7	-2.97	-0.80	2.17
7A		15.8	-2.97	-0.80	2.17						

[a] Single point energies were calculated using single crystal structures without optimization and replacing Ag with Cu atoms directly. [b] Not applicable.

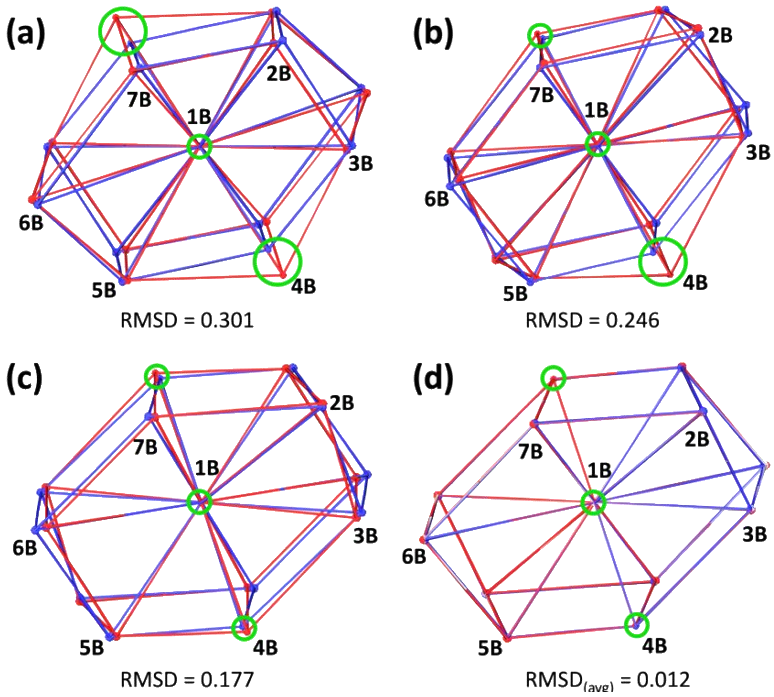

Fig. S24. (a-c) Overlay of (red) initial guess $\mathbf{Ag_{11.3}Cu_{1.7}}$ single crystal and (blue) optimized $\mathbf{Ag_{10}Cu_3}$ structures (only 13-metal cores shown here) to determine the possible positions of foreign Cu atoms due to Ag/Cu structural disorder. (a) initial guess: both position 4B and 4B' were Ag atoms in single crystal but set as Cu atoms; (b) initial guess: position 4B was Ag atom and position 4B' (not shown) was Cu atom in single crystal but both positions were set as Cu atoms; (c) initial guess: both position 4B and 4B' were Cu atoms in single crystal and remained in optimization. Green-circled positions are copper atoms. (d) Overlay of three optimized structures from three different initial guesses. Root mean square displacement/deviation (RMSD) is an effective index to show the differences between two or more structures, closer to 0 meaning more similar structures. As shown in this figure, we can see no matter which initial guess was adopted to construct $\mathbf{Ag_{10}Cu_3}$ cluster, the full-optimized structures would be close to each other (average RMSD = 0.012) and correspond to Cu disordering positions in single crystallographic study (RMSD(c) = 0.177, smaller than other two values).

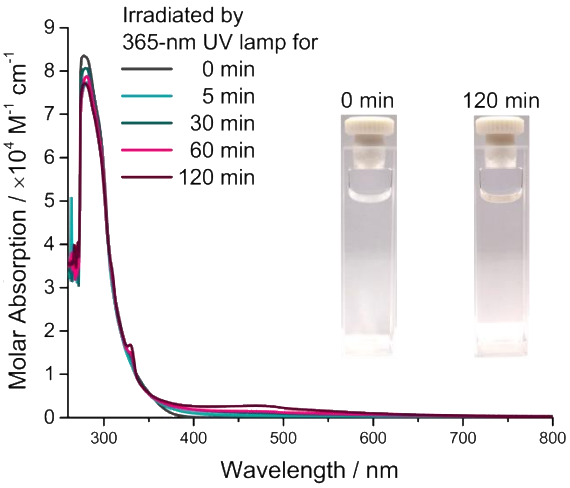

Fig. S25. Time-dependent UV-vis spectra of Ag_{13} in benzene solution after irradiated by 365-nm UV lamp. Inserted digital pictures correspond to fresh solution before and after irradiated for 120 minutes, respectively.

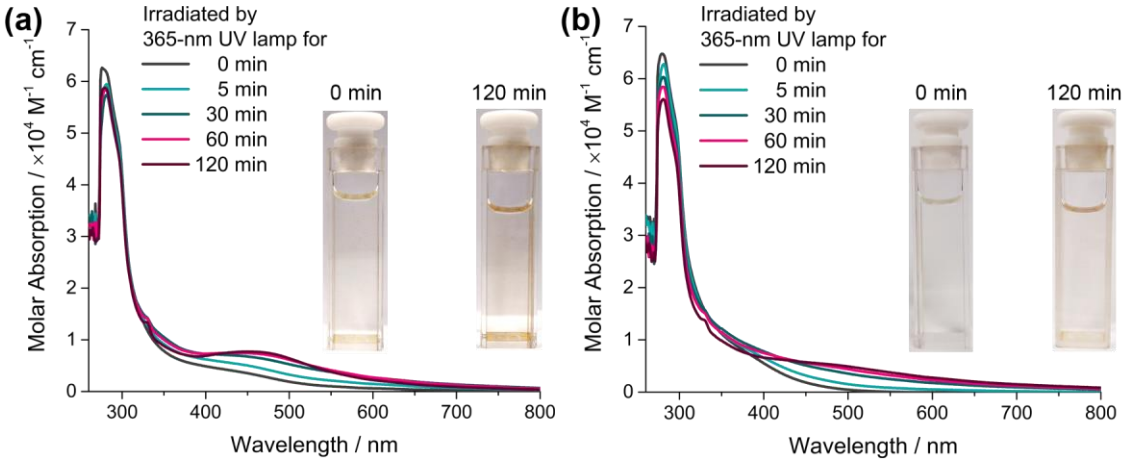

Fig. S26. Time-dependent UV-vis spectra of (a) $Ag_{11.8}Cu_{1.2}$ and (b) $Ag_{11.3}Cu_{1.7}$ in benzene solution after irradiated by 365-nm UV lamp. Inserted digital pictures correspond to fresh solution before and after irradiated for 120 minutes, respectively.

Comments: we found fresh solution could be stable under sunlight or indoor light environment. Once measuring emission spectra of these solutions and keeping excited by high-energy ultraviolet light, the colour of solution turned darker relative to fresh solution. We suspected that both silver cluster and heterometallic Ag/Cu cluster underwent photo-reduction into Ag(0) or heterometallic Ag(0)/Cu(0) species due to low-energy absorption. The same phenomena were also reported by Omary *et al.* (*J. Am. Chem. Soc.* **2007**, *129*, 11384-11393) and Petty, Lieberman *et al.* (*J. Am. Chem. Soc.* **2019**, *141*, 11465-11470), which photo-sensitive metal complexes would suffer photoreduction to show darker colours. Due to this, in this work, all photophysics study were performed on crystalline sample of clusters. Further study on photoreduction of these metal clusters are undergoing.

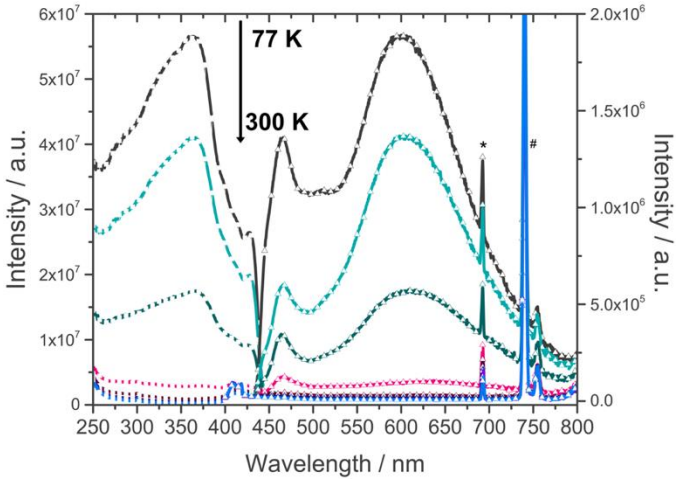

Fig. S27. Varied-temperature excitation-emission spectra of Ag_{13} in solid state. Excitation spectra (-□-) were recorded under the emission of 600 nm and emission spectra (-Δ-) were recorded under the excitation of 370 nm. Asterisk (*) and number sign (#) mean the instrumental error and double frequency signals, respectively.

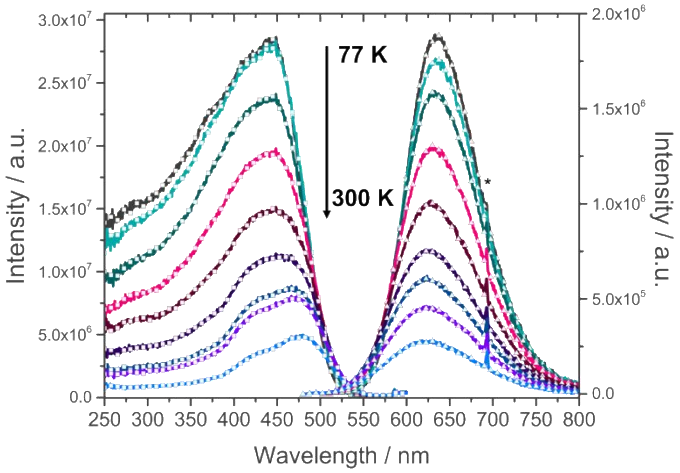

Fig. S28. Varied-temperature excitation-emission spectra of $Ag_{11.8}Cu_{1.2}$ in solid state. Excitation spectra (-□-) was recorded under the emission of 630 nm and emission spectra (-Δ-) were recorded under the excitation of 450 nm. Asterisk (*) means the instrumental error.

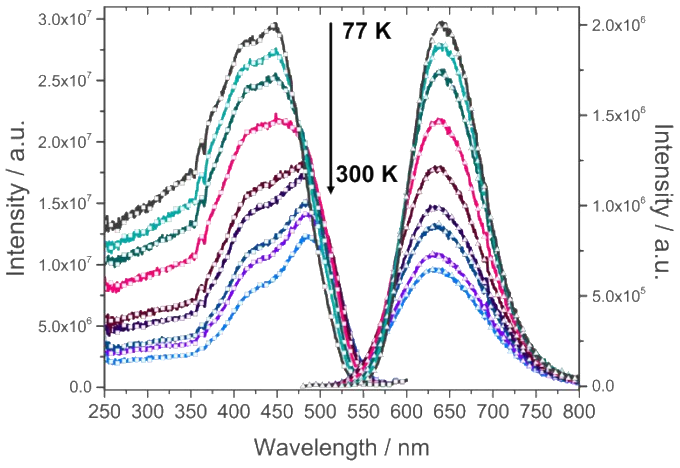

Fig. S29. Varied-temperature excitation-emission spectra of $Ag_{11.3}Cu_{1.7}$ in solid state. Excitation spectra (-□-) was recorded under the emission of 630 nm and emission spectra (-Δ-) were recorded under the excitation of 450 nm.

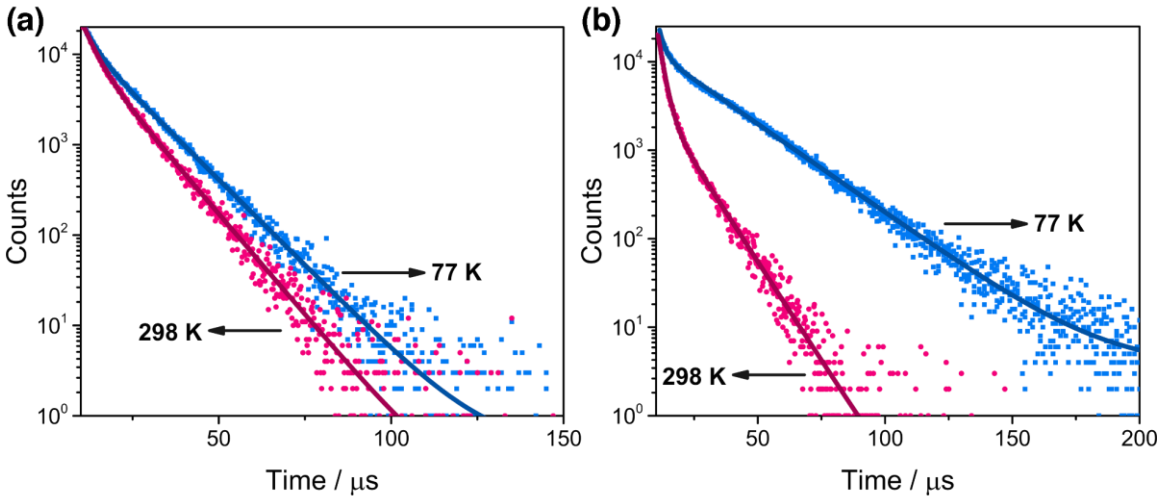

Fig. S30. Photoluminescence decay and fitting curves of (a) $Ag_{11.8}Cu_{1.2}$ and (b) $Ag_{11.3}Cu_{1.7}$ under 298 K and 77 K.

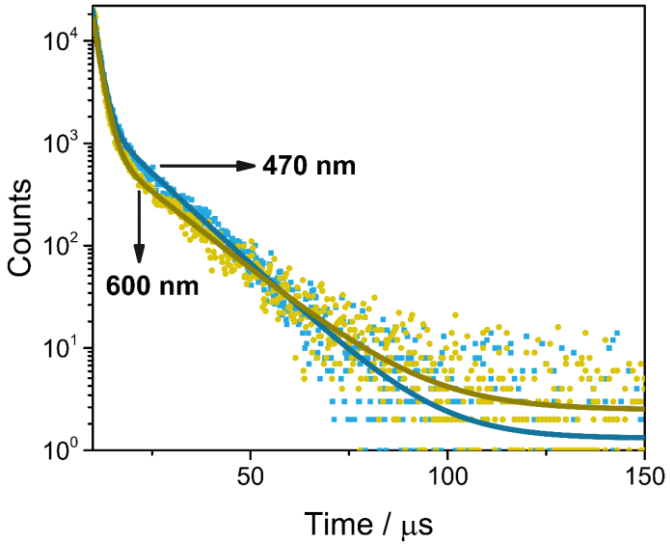

Fig. S31. Photoluminescence decay and fitting curves of Ag_{13} under 77 K. Monitored emissions are 470 nm and 600 nm, respectively.

Table S5. Photoluminescence lifetime data for all nanoclusters in solid states.

Nanoclusters	Temperature / K	Emission / nm	A_1	τ_1 / μs	A_2	τ_2 / μs	τ_{av} / μs[a]	R^2
Ag_{13}	298	~460	-	-	-	-	-[b]	-
	77	465	10779.8	1.58	1643.1	12.20	7.32	0.9999
		600	10759.1	1.74	916.6	14.22	6.86	0.9999
$Ag_{11.8}Cu_{1.2}$	298	623	13372.7	3.58	10430.8	9.73	7.76	0.9999
	77	635	15595.7	3.36	15283.2	11.46	9.59	0.9999
$Ag_{11.3}Cu_{1.7}$	298	632	19427.8	2.19	3215.9	9.72	5.38	0.9999
	77	640	9804.1	1.97	11615.2	21.64	20.24	0.9999

[a] $\tau_{av} = (A_1\times\tau_1^2+A_2\times\tau_2^2)/(A_1\times\tau_1+A_2\times\tau_2)$. [b] The emission of Ag_{13} is too faint to measure lifetime.

Table S6. Absolute photoluminescence quantum yields (Φ_{PL})[a] for all nanoclusters in solid states.

Nanoclusters	Temperature / K	Area of Excitation Light (Blank)	Area of Excitation Light (Sample)	Area of Absorbance Light (Sample)[b]	Area of Emission Light (Sample)	Φ_{PL}[c] / %	$\Phi_{PL\ (avg.)}$ / %
Ag_{13}	298	644618811	334496760	310122051	1269620	0.41	0.45 ± 0.06
		667266153	347665420	319600733	1494141	0.47	
		613149884	388112697	225037187	1071866	0.48	
		625028935	354921713	270107222	1403782	0.52	
		678919563	388967500	289952063	1043511	0.36	
	77	203750944	193654775	10096169	7629823	75.57	74.28 ± 2.04
		216177406	205831939	10345467	7827288	75.66	
		248459715	238551109	9908606	7501758	75.71	
		287084388	275745045	11339343	8317555	73.35	
		284391553	275887153	8504400	6045845	71.09	
$Ag_{11.8}Cu_{1.2}$	298	388670336	338330539	50339797	31910641	63.39	63.29 ± 3.36
		541955703	382908254	159047449	96492277	60.67	
		487340037	406026730	81313307	53683519	66.02	
		404938631	313799298	91139333	54013948	59.27	
		474716889	359691799	115025090	77211489	67.13	
	77	372255857	343995489	28260368	28411767	100.54	99.23 ± 1.74
		374411258	352146396	22264862	21979171	98.72	
		331125580	314684145	16441435	15905626	96.74	
		327932303	316902763	11029540	10912907	98.94	
		370941149	353792751	17148398	17353122	101.19	
$Ag_{11.3}Cu_{1.7}$	298	446230765	349657475	96573290	57568396	59.61	61.02 ± 0.95
		520681125	309662217	211018908	128219045	60.76	
		426851659	240311067	186540592	113866943	61.04	
		409790236	266411336	143378900	88248417	61.55	
		393224412	292606052	100618360	62530050	62.15	
	77	388391039	345688730	42702309	41627990	97.48	98.45 ± 1.62
		343268578	310237415	33031163	33372867	101.03	
		285523007	271668801	13854206	13511936	97.53	
		267499634	259564621	7935013	7860383	99.06	
		256706743	252760381	3946362	3833888	97.15	

[a] All data are from five different batches of prepared samples to ensure the reproducibility. [b] Area of absorbance light (sample) = Area of excitation light (blank) – Area of excitation light (sample). [c] Φ_{PL} = [Area of emission light (sample)] / [Area of absorbance light (sample)] × 100%.

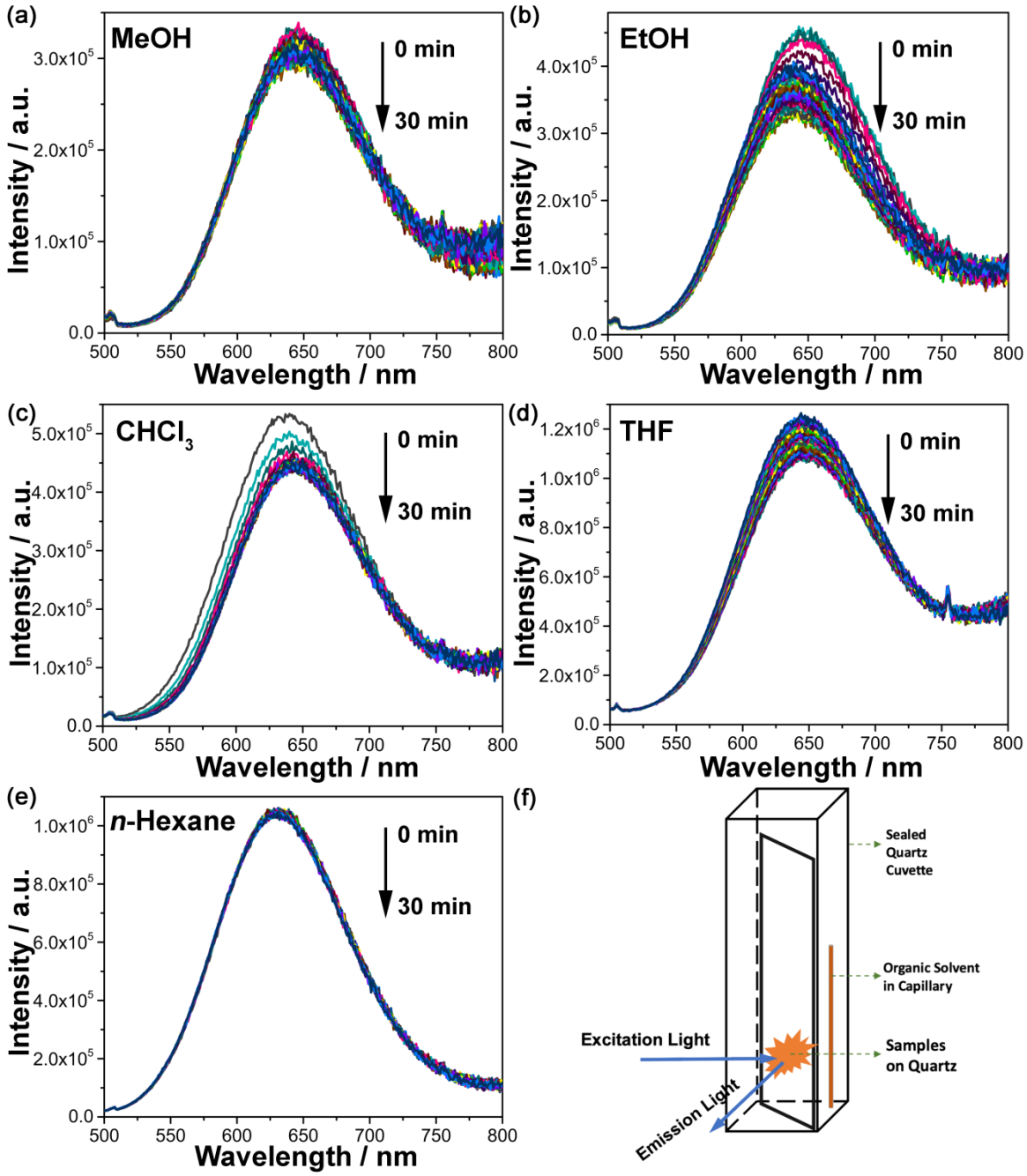

Fig. S32. Real-time emission spectra of solid-state $Ag_{11.8}Cu_{1.2}$ contacting with different organic solvent vapors, (a) MeOH, (b) EtOH, (c) $CHCl_3$, (d) THF, and (e) *n*-Hexane. (f) Experimental setup for the solid-gas detection. (*Chem. Sci.* **2013**, *4*, 1793-1801)

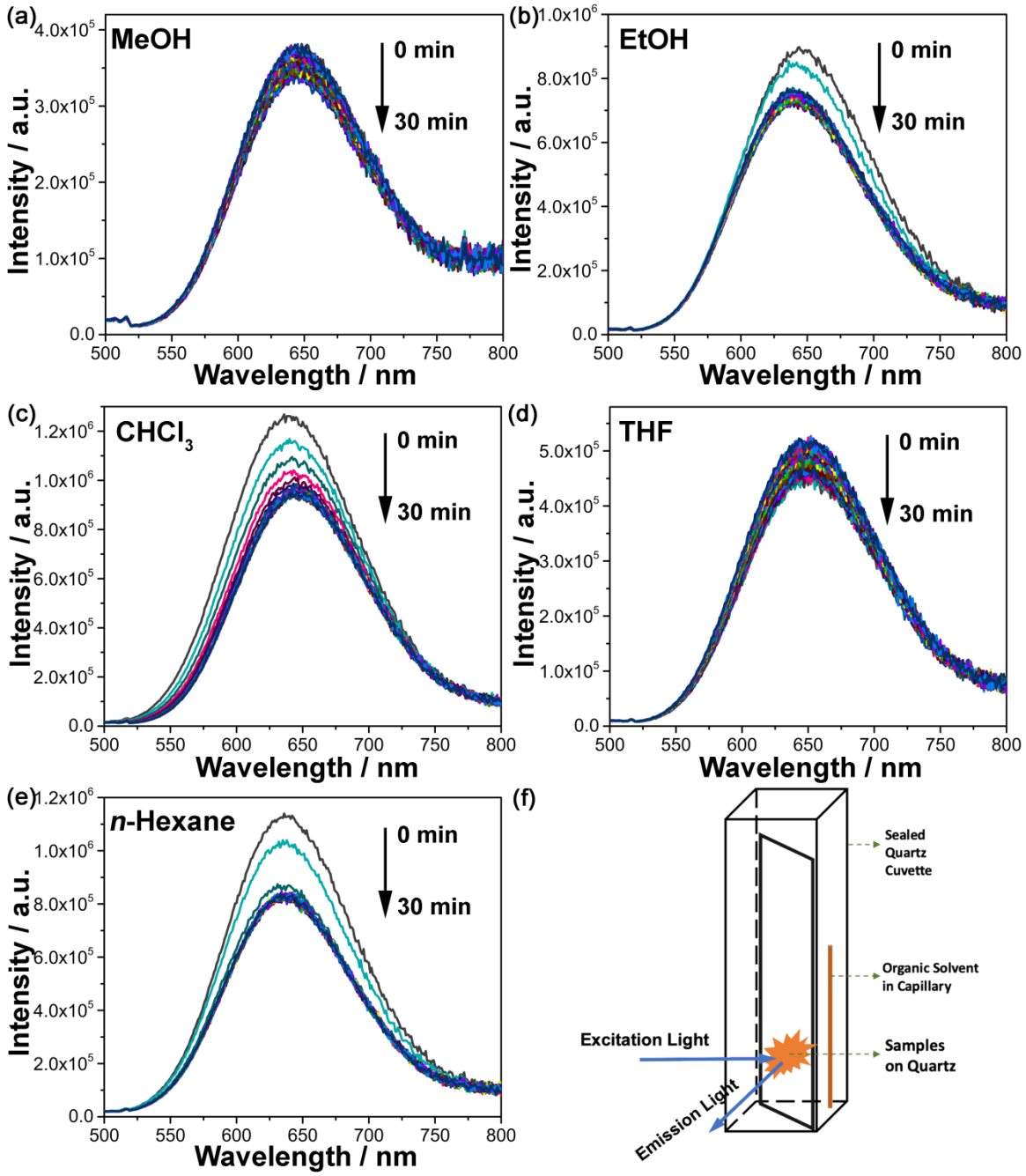

Fig. S33. Real-time emission spectra of solid-state $Ag_{11.3}Cu_{1.7}$ contacting with different organic solvent vapors, (a) MeOH, (b) EtOH, (c) $CHCl_3$, (d) THF, and (e) *n*-Hexane. (f) Experimental setup for the solid-gas detection. (*Chem. Sci.* **2013**, *4*, 1793-1801)

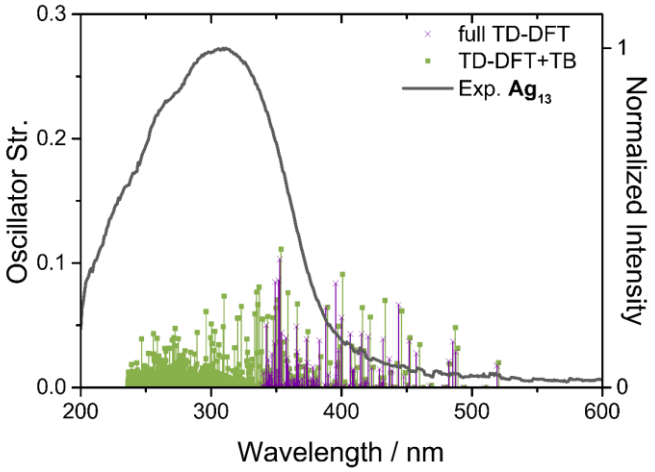

Fig. S34. Absorption spectrum of Ag_{13} nanocluster calculated by (purple) full TD-DFT method and (green) TD-DFT+TB approximation. Solid line represents experimental absorption spectrum in solid state.

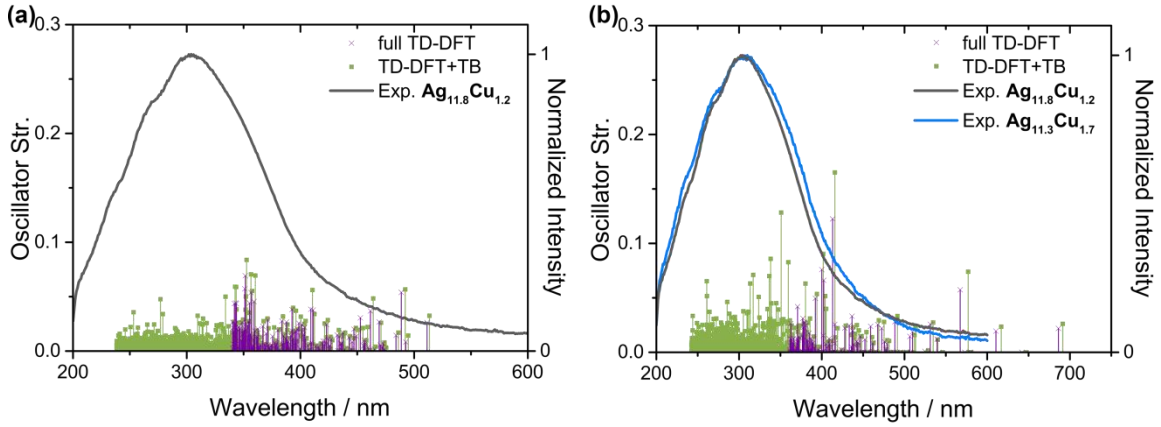

Fig. S35. Absorption spectra of (a) **[Cu@Ag_{12}]** and (b) **[Cu@$Ag_{10}Cu_2$]** nanoclusters calculated by (purple) full TD-DFT method and (green) TD-DFT+TB approximation. Solid lines represent experimental absorption spectra to responding copper/silver bimetallic nanoclusters in solid state.

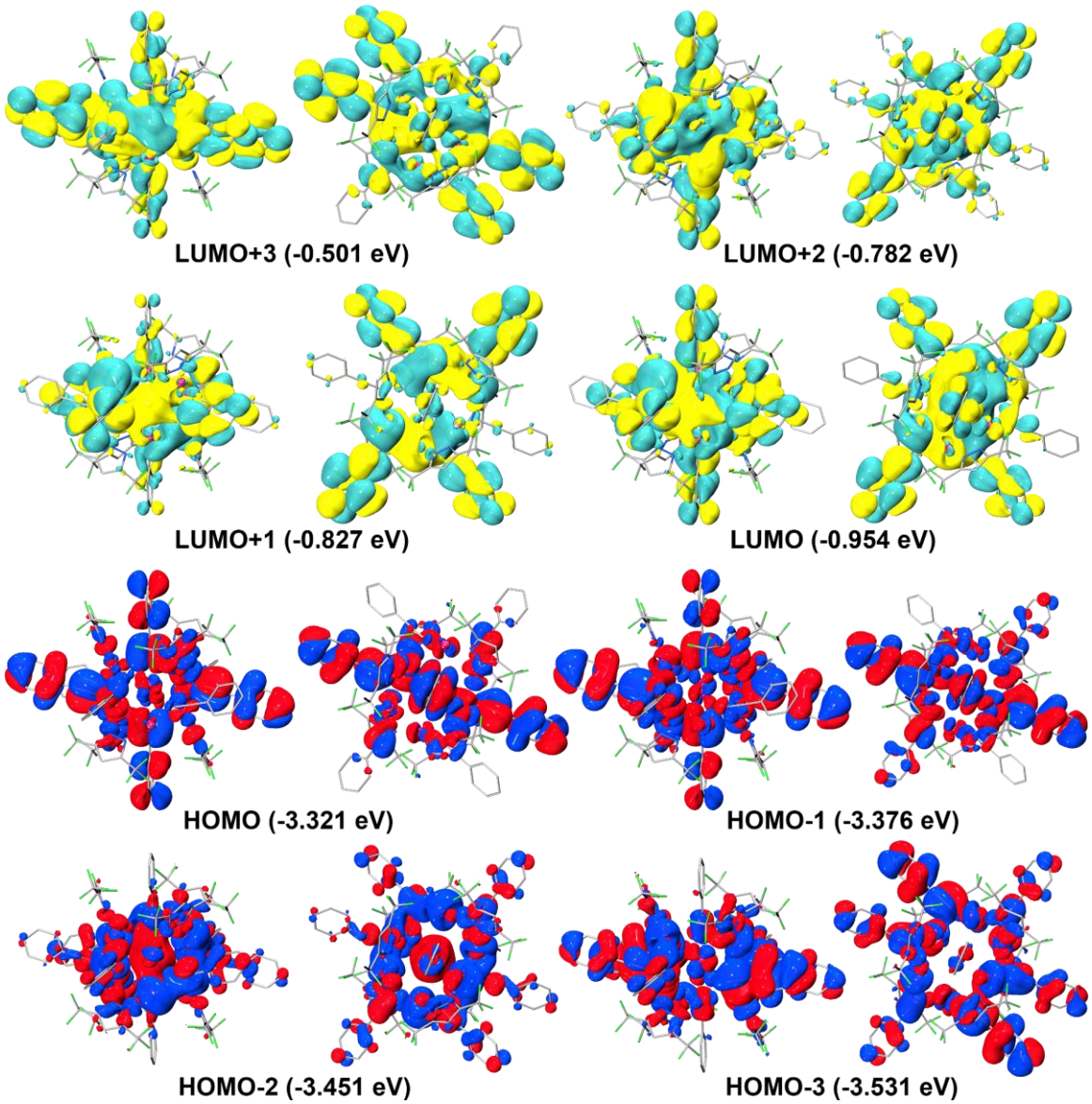

Fig. S36. Frontier molecular orbitals of Ag_{13} (isovalue = 0.01 a.u., left: side view, right: top view).

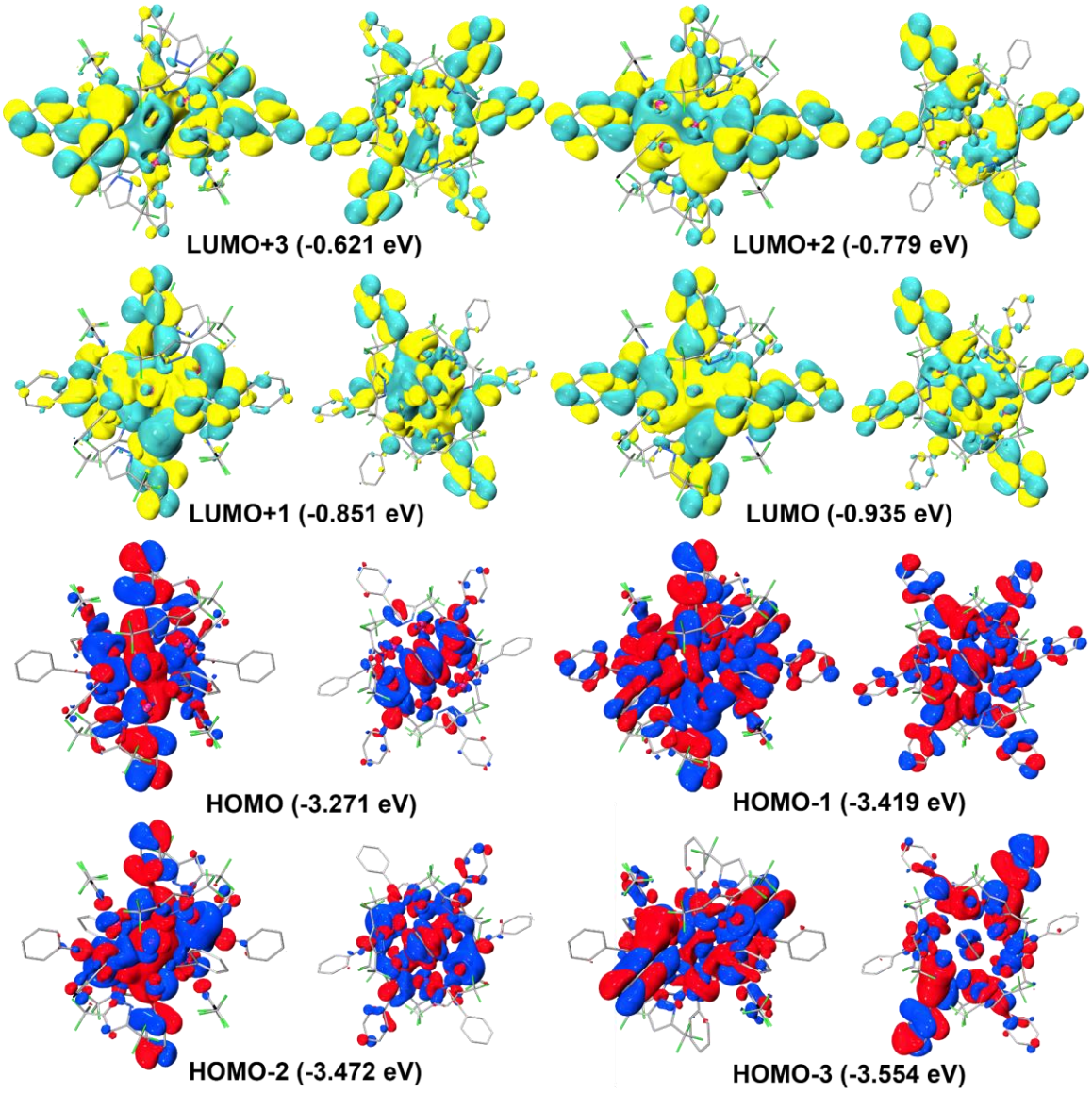

Fig. S37. Frontier molecular orbitals of **[Cu@Ag_{12}]** (isovalue = 0.01 a.u., left: side view, right: top view).

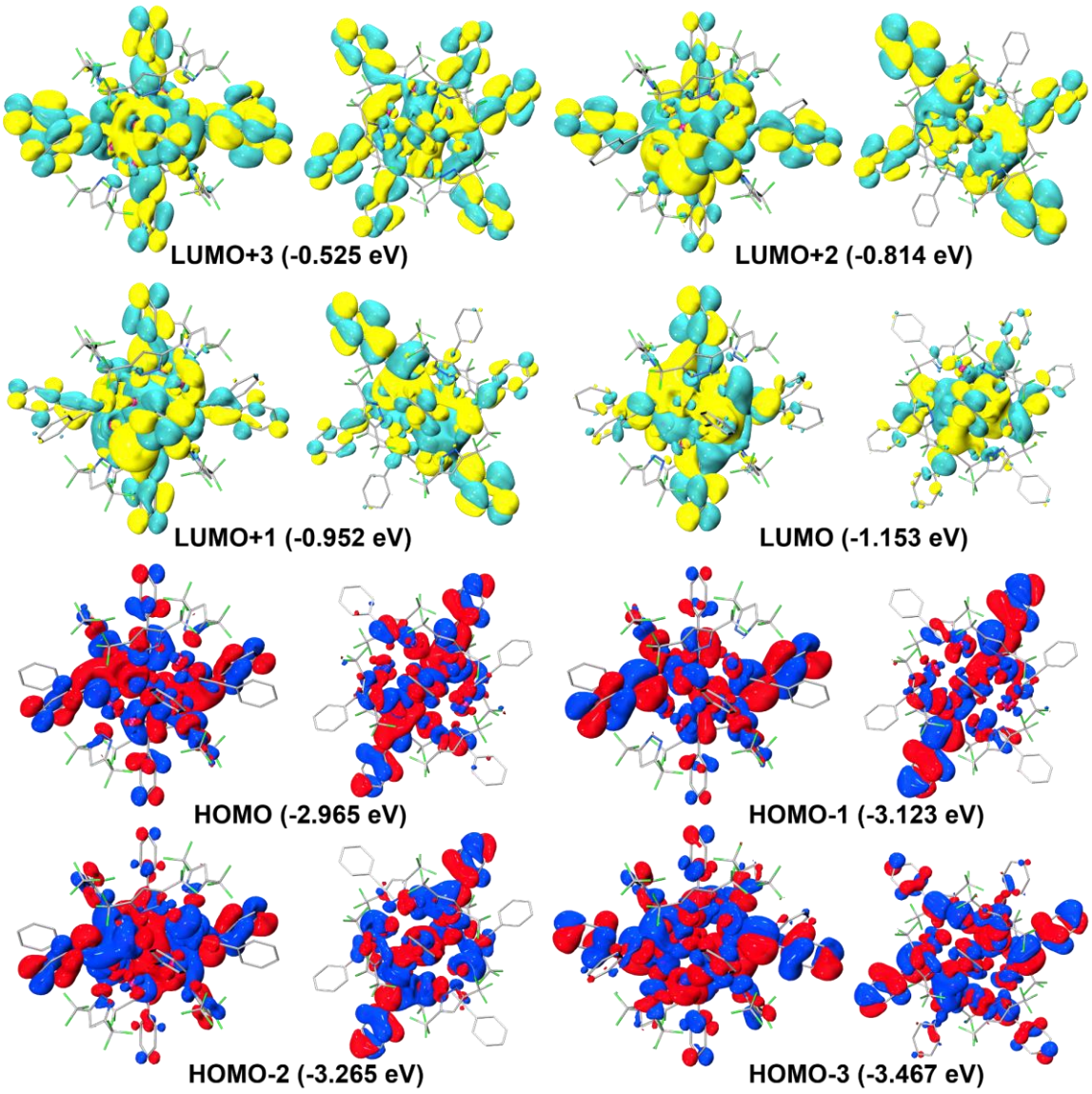

Fig. S38. Frontier molecular orbitals of **[Cu@$Ag_{10}Cu_2$]** (isovalue = 0.01 a.u., left: side view, right: top view).

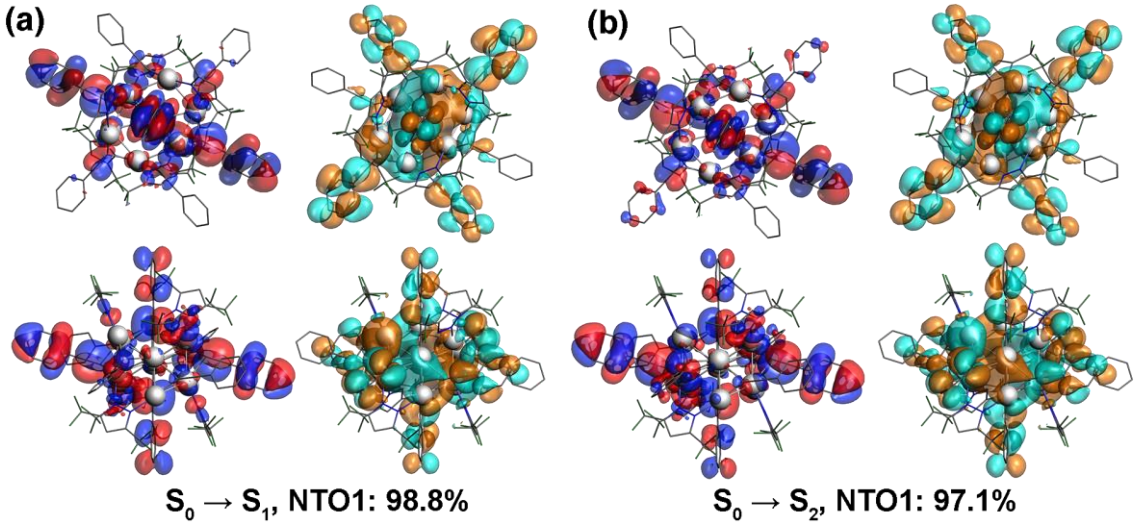

Fig. S39. Natural transition orbitals (NTOs) for S_1 and S_2 of **Ag_{13}** (isovalue = 0.01 a.u., upper: top view, bottom: side view).

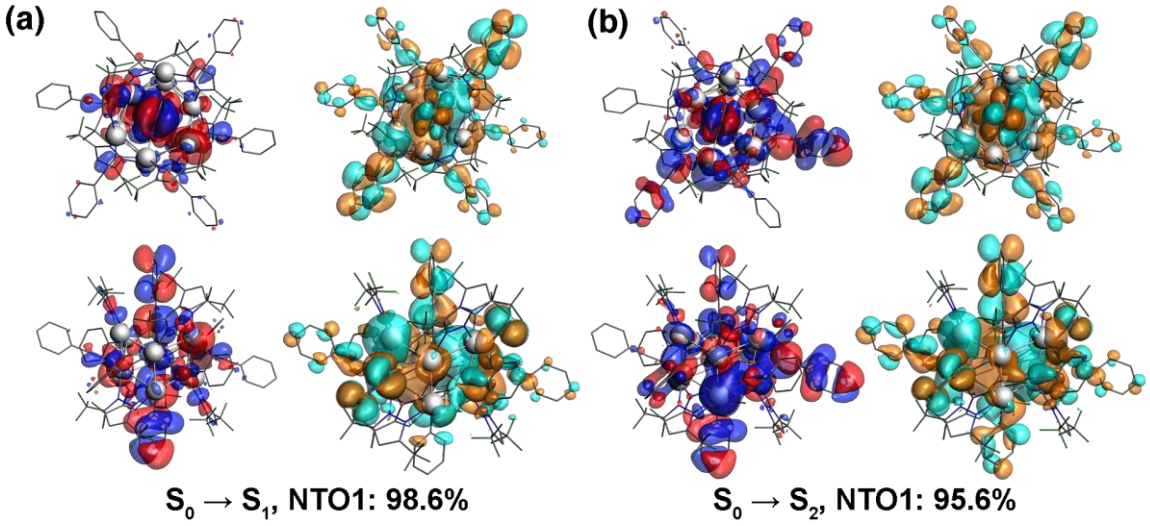

Fig. S40. Natural transition orbitals (NTOs) for S_1 and S_2 of **[Cu@Ag_{12}]** (isovalue = 0.01 a.u., upper: top view, bottom: side view).

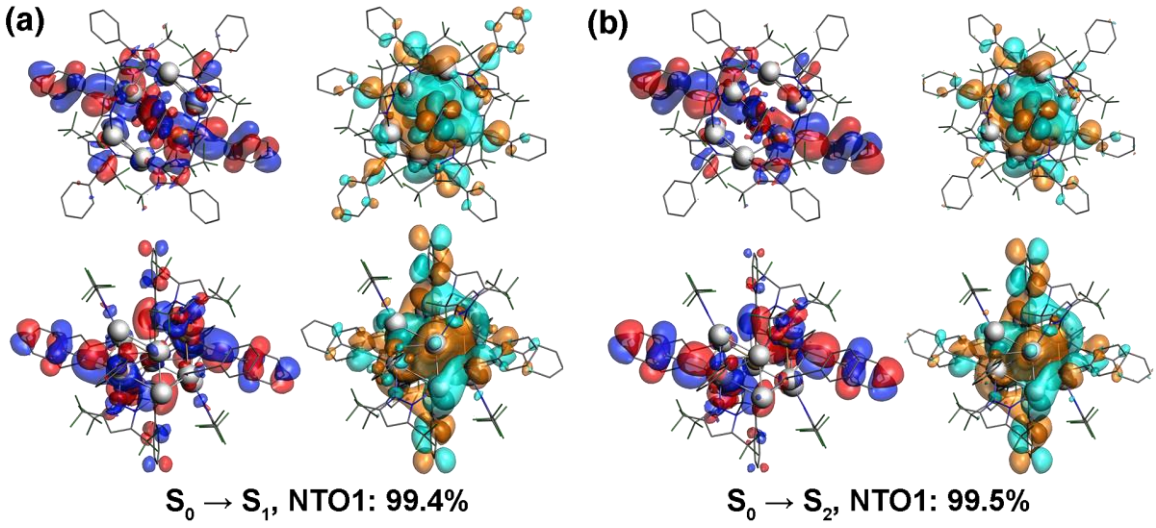

Fig. S41. Natural transition orbitals (NTOs) for S_1 and S_2 of **[Cu@$Ag_{10}Cu_2$]** (isovalue = 0.01 a.u., upper: top view, bottom: side view).

Table S7. Selected bond lengths (Å) and bond angles (°) of **Ag_{13}**.

Ag(03)-Ag(06)#1	3.3283(4)	Ag(02)-Ag(04)	3.0049(3)	Ag(03)-N(6)	2.275(3)
Ag(03)-Ag(04)	3.3128(4)	Ag(01)-Ag(02)#1	2.9133(2)	Ag(06)-C(6)	2.275(3)
Ag(02)-Ag(05)	3.2917(3)	Ag(01)-Ag(02)	2.9133(2)	Ag(06)-N(2)	2.261(3)
Ag(06)-Ag(07)	3.2616(4)	Ag(04)-Ag(06)#1	2.8655(4)	Ag(03)-C(24)	2.253(3)
Ag(01)-Ag(03)#1	3.1607(3)	Ag(03)-Ag(05)#1	2.8451(4)	Ag(07)-N(1)	2.178(3)
Ag(01)-Ag(03)	3.1607(2)	Ag(03)-Ag(07)	2.8386(4)	Ag(07)-C(24)	2.125(4)
Ag(01)-Ag(06)#1	3.1606(3)	Ag(02)-C(46)	2.566(3)	Ag(05)-N(3)	2.112(3)
Ag(01)-Ag(06)	3.1606(3)	Ag(02)-C(24)#1	2.425(3)	Ag(04)-N(5)	2.109(3)
Ag(05)-Ag(06)	3.1346(4)	Ag(06)-C(32)#1	2.364(3)	Ag(05)-C(6)	2.080(3)
Ag(01)-Ag(07)#1	3.1071(3)	Ag(02)-C(32)	2.361(3)	Ag(04)-C(32)	2.067(3)
Ag(01)-Ag(07)	3.1070(3)	Ag(03)-C(6)#1	2.321(3)	Ag(01)-C(46)	2.038(3)
Ag(02)-Ag(07)#1	3.0817(4)	Ag(02)-N(4)	2.281(3)	Ag(01)-C(46)#1	2.038(3)
Ag(02)#1-Ag(01)-Ag(02)	180	Ag(02)#1-Ag(01)-Ag(07)#1	118.523(8)	Ag(07)-Ag(01)-Ag(06)	62.711(7)
Ag(02)-Ag(01)-Ag(03)#1	70.906(7)	Ag(03)-Ag(01)-Ag(03)#1	180	Ag(07)#1-Ag(01)-Ag(06)	117.289(7)
Ag(02)#1-Ag(01)-Ag(03)#1	109.095(7)	Ag(03)-Ag(01)-Ag(06)#1	63.541(6)	Ag(07)#1-Ag(01)-Ag(06)#1	62.712(7)
Ag(02)#1-Ag(01)-Ag(03)	70.905(7)	Ag(06)-Ag(01)-Ag(03)#1	63.542(6)	Ag(07)-Ag(01)-Ag(07)#1	180
Ag(02)-Ag(01)-Ag(03)	109.094(7)	Ag(06)#1-Ag(01)-Ag(03)#1	116.459(6)	Ag(01)-Ag(02)-Ag(04)	77.218(7)
Ag(02)-Ag(01)-Ag(06)#1	77.201(7)	Ag(06)-Ag(01)-Ag(03)	116.458(6)	Ag(01)-Ag(02)-Ag(05)	80.890(8)
Ag(02)#1-Ag(01)-Ag(06)#1	102.800(7)	Ag(06)-Ag(01)-Ag(06)#1	180	Ag(01)-Ag(02)-Ag(07)#1	62.359(8)
Ag(02)-Ag(01)-Ag(06)	102.800(7)	Ag(07)-Ag(01)-Ag(03)	53.852(7)	Ag(04)-Ag(02)-Ag(05)	135.994(10)
Ag(02)#1-Ag(01)-Ag(06)	77.200(7)	Ag(07)-Ag(01)-Ag(03)#1	126.148(7)	Ag(04)-Ag(02)-Ag(07)#1	103.500(10)
Ag(02)-Ag(01)-Ag(07)#1	61.478(8)	Ag(07)#1-Ag(01)-Ag(03)	126.148(7)	Ag(07)#1-Ag(02)-Ag(05)	99.257(10)
Ag(02)-Ag(01)-Ag(07)	118.522(8)	Ag(07)#1-Ag(01)-Ag(03)#1	53.852(7)	Ag(01)-Ag(03)-Ag(04)	69.538(7)
Ag(02)#1-Ag(01)-Ag(07)	61.477(8)	Ag(07)-Ag(01)-Ag(06)#1	117.288(7)	Ag(01)-Ag(03)-Ag(06)#1	58.228(6)
Ag(07)-Ag(03)-Ag(01)	62.109(8)	Ag(02)-Ag(04)-Ag(03)	103.057(9)	Ag(04)-Ag(03)-Ag(06)#1	51.123(7)
Ag(07)-Ag(03)-Ag(04)	104.511(11)	Ag(06)#1-Ag(04)-Ag(02)	80.496(9)	Ag(05)#1-Ag(03)-Ag(01)	84.261(8)
Ag(07)-Ag(03)-Ag(05)#1	117.437(11)	Ag(06)#1-Ag(04)-Ag(03)	64.718(9)	Ag(05)#1-Ag(03)-Ag(04)	110.808(10)
Ag(07)-Ag(03)-Ag(06)#1	120.225(11)	Ag(03)#1-Ag(05)-Ag(02)	69.770(9)	Ag(05)#1-Ag(03)-Ag(06)#1	60.427(8)

Ag(03)#1-Ag(05)-Ag(06)	67.441(9)	Ag(01)-Ag(06)-Ag(03)#1	58.231(6)	Ag(01)-Ag(06)-Ag(07)	57.841(7)
Ag(01)-Ag(07)-Ag(06)	59.448(7)	Ag(06)-Ag(05)-Ag(02)	95.272(9)	Ag(04)#1-Ag(06)-Ag(01)	75.430(8)
Ag(04)#1-Ag(06)-Ag(03)#1	64.158(9)	Ag(04)#1-Ag(06)-Ag(05)	115.483(11)	Ag(04)#1-Ag(06)-Ag(07)	102.358(10)
Ag(02)#1-Ag(07)-Ag(06)	73.415(9)	Ag(02)#1-Ag(07)-Ag(01)	56.164(7)	Ag(03)-Ag(07)-Ag(01)	64.040(8)
Ag(03)-Ag(07)-Ag(02)#1	73.046(9)	Ag(03)-Ag(07)-Ag(06)	123.367(12)	Ag(05)-Ag(06)-Ag(01)	79.742(8)
Ag(05)-Ag(06)-Ag(03)#1	52.132(8)	Ag(05)-Ag(06)-Ag(07)	112.486(11)	Ag(07)-Ag(06)-Ag(03)#1	115.988(10)
C(46)#1-Ag(01)-Ag(02)	120.66(8)	C(46)-Ag(02)-Ag(01)	43.08(7)	C(6)#1-Ag(03)-Ag(05)#1	46.11(8)
C(46)-Ag(01)-Ag(02)#1	120.67(8)	C(46)-Ag(02)-Ag(04)	69.22(7)	C(6)#1-Ag(03)-Ag(06)#1	43.05(8)
C(46)-Ag(01)-Ag(02)	59.33(8)	C(46)-Ag(02)-Ag(05)	68.67(7)	C(6)#1-Ag(03)-Ag(07)	158.41(8)
C(46)#1-Ag(01)-Ag(02)#1	59.34(8)	C(46)-Ag(02)-Ag(07)#1	105.24(8)	C(24)-Ag(03)-Ag(01)	87.24(8)
C(46)#1-Ag(01)-Ag(03)	100.51(9)	C(32)-Ag(02)-Ag(01)	90.53(8)	C(24)-Ag(03)-Ag(04)	151.12(9)
C(46)-Ag(01)-Ag(03)#1	100.51(9)	C(32)-Ag(02)-Ag(04)	43.27(8)	C(24)-Ag(03)-Ag(05)#1	82.54(9)
C(46)-Ag(01)-Ag(03)	79.49(9)	C(32)-Ag(02)-Ag(05)	170.89(8)	C(24)-Ag(03)-Ag(06)#1	129.64(9)
C(46)#1-Ag(01)-Ag(03)#1	79.49(9)	C(32)-Ag(02)-Ag(07)#1	73.83(8)	C(24)-Ag(03)-Ag(07)	47.65(9)
C(46)#1-Ag(01)-Ag(06)#1	71.89(9)	C(32)-Ag(02)-C(46)	106.96(10)	C(24)-Ag(03)-N(6)	120.45(11)
C(46)-Ag(01)-Ag(06)#1	108.11(9)	C(32)-Ag(02)-C(24)#1	106.22(11)	C(24)-Ag(03)-C(6)#1	126.60(13)
C(46)#1-Ag(01)-Ag(06)	108.11(9)	C(24)#1-Ag(02)-Ag(01)	90.05(8)	C(32)-Ag(04)-Ag(02)	51.52(8)
C(46)-Ag(01)-Ag(06)	71.89(9)	C(24)#1-Ag(02)-Ag(04)	145.57(9)	C(32)-Ag(04)-Ag(03)	115.79(9)
C(46)#1-Ag(01)-Ag(07)	120.53(8)	C(24)#1-Ag(02)-Ag(05)	70.96(8)	C(32)-Ag(04)-Ag(06)#1	54.40(9)
C(46)-Ag(01)-Ag(07)	59.47(8)	C(24)#1-Ag(02)-Ag(07)#1	43.40(9)	C(32)-Ag(04)-N(5)	171.67(11)
C(46)#1-Ag(01)-Ag(07)#1	59.47(8)	C(24)#1-Ag(02)-C(46)	121.14(11)	C(6)-Ag(05)-Ag(02)	119.19(9)
C(46)-Ag(01)-Ag(07)#1	120.53(8)	C(6)#1-Ag(03)-Ag(01)	98.90(8)	C(6)-Ag(05)-Ag(03)#1	53.54(9)
C(46)#1-Ag(01)-C(46)	180	C(6)#1-Ag(03)-Ag(04)	75.58(8)	C(6)-Ag(05)-Ag(06)	46.49(9)
C(6)-Ag(06)-Ag(01)	99.96(8)	C(6)-Ag(06)-Ag(03)#1	44.15(8)	C(6)-Ag(05)-N(3)	173.83(12)
C(6)-Ag(06)-Ag(04)#1	86.26(9)	C(6)-Ag(06)-Ag(05)	41.53(8)	C(6)-Ag(06)-Ag(07)	151.94(8)
C(6)-Ag(06)-C(32)#1	128.87(12)	C(32)#1-Ag(06)-Ag(01)	84.66(7)	C(32)#1-Ag(06)-Ag(03)#1	106.77(8)
C(32)#1-Ag(06)-Ag(04)#1	45.31(8)	C(32)#1-Ag(06)-Ag(05)	158.44(8)	C(32)#1-Ag(06)-Ag(07)	70.25(7)
C(24)-Ag(07)-Ag(01)	90.91(9)	C(24)-Ag(07)-Ag(02)#1	51.61(9)	C(24)-Ag(07)-Ag(03)	51.57(9)
C(24)-Ag(07)-Ag(06)	124.55(9)	C(24)-Ag(07)-N(1)	146.80(11)	N(4)-Ag(02)-Ag(01)	130.34(7)
N(4)-Ag(02)-Ag(04)	107.33(7)	N(4)-Ag(02)-C(32)	127.37(10)	N(6)-Ag(03)-Ag(01)	116.15(7)
N(4)-Ag(02)-Ag(05)	61.46(7)	N(4)-Ag(02)-C(24)#1	105.26(11)	N(6)-Ag(03)-Ag(04)	60.46(7)
N(4)-Ag(02)-Ag(07)#1	148.65(7)	N(6)-Ag(03)-Ag(07)	94.16(7)	N(6)-Ag(03)-Ag(05)#1	148.19(7)
N(4)-Ag(02)-C(46)	90.97(10)	N(6)-Ag(03)-C(6)#1	104.10(11)	N(6)-Ag(03)-Ag(06)#1	108.05(7)
N(5)-Ag(04)-Ag(02)	136.70(7)	N(2)-Ag(06)-Ag(01)	114.20(6)	N(2)-Ag(06)-Ag(05)	98.28(7)
N(5)-Ag(04)-Ag(03)	66.31(8)	N(2)-Ag(06)-Ag(03)#1	149.25(7)	N(2)-Ag(06)-Ag(07)	63.40(7)
N(5)-Ag(04)-Ag(06)#1	123.89(8)	N(2)-Ag(06)-Ag(04)#1	146.20(7)	N(2)-Ag(06)-C(6)	121.24(11)
N(2)-Ag(06)-C(32)#1	101.67(10)	N(1)-Ag(07)-Ag(01)	117.65(7)	N(1)-Ag(07)-Ag(02)#1	130.17(7)
N(1)-Ag(07)-Ag(03)	154.98(7)	N(1)-Ag(07)-Ag(06)	65.69(7)		

Symmetry transformations used to generate equivalent atoms:

#1 -x+1,-y+1,-z+1

Table S8. Selected bond lengths (Å) and bond angles (°) of $Ag_{11.8}Cu_{1.2}$.

Ag(02)-Ag(04)	3.3071(10)	Ag(01)-Ag(06)#1	3.0537(10)	Ag(04)-Ag(06)#1	2.8371(13)
Ag(01)-Ag(05)	3.3000(12)	Ag(02)-Ag(05)	3.0498(12)	Ag(02)-Cu(0A)	3.1018(9)

Ag(03)-Ag(04)	3.2982(12)	Ag(01)-Ag(03)#1	3.0232(12)	Ag(04)-Ag(07)	3.0857(10)
Ag(02)-Ag(06)	3.2708(13)	Ag(02)-Ag(03)	2.8728(11)	Ag(04)-Cu(0A)	3.0857(10)
Ag(02)-Ag(07)	3.1018(9)	Ag(04)-Ag(05)	2.8660(11)	Ag(01)-Ag(06)#1	3.0537(10)
Ag(04)-Ag(07)	3.0857(10)	Ag(01)-Ag(07)	2.8551(7)	Ag(02)-Ag(05)	3.0498(12)
Ag(01)-C(012)	2.538(10)	Ag(04)-C(1)#1	2.282(10)	Ag(01)-N(00J)	2.293(8)
Ag(01)-C(1)#1	2.422(10)	Ag(02)-C(01L)	2.246(11)	Ag(04)-N(00Q)	2.270(8)
Ag(02)-C(013)	2.383(11)	Ag(06)-C(1)	2.098(10)	Ag(02)-N(00D)	2.267(7)
Ag(01)-C(013)#1	2.365(12)	Ag(03)-C(013)	2.078(9)	Ag(06)-N(00F)	2.127(9)
Ag(04)-C(01L)	2.345(10)	Ag(05)-C(01L)	2.074(12)	Ag(05)-N(00E)	2.123(9)
Ag(07)-C(012)	1.931(11)	Ag(07)-C(012)#1	1.931(11)	Ag(03)-N(00P)	2.116(8)
Ag(03)#1-Ag(01)-Ag(05)	136.90(3)	Ag(05)-Ag(02)-Ag(04)	53.41(2)	Ag(06)#1-Ag(04)-Ag(02)	123.99(4)
Ag(03)#1-Ag(01)-Ag(06)#1	107.25(3)	Ag(05)-Ag(02)-Ag(07)	78.92(3)	Ag(06)#1-Ag(04)-Ag(03)	112.95(4)
Ag(07)-Ag(01)-Ag(03)#1	81.09(3)	Ag(06)-Ag(02)-Ag(04)	118.40(3)	Ag(07)-Ag(04)-Ag(02)	57.93(2)
Ag(07)-Ag(01)-Ag(05)	78.51(2)	Ag(07)-Ag(02)-Ag(04)	57.46(2)	Ag(07)-Ag(04)-Ag(03)	73.50(3)
Ag(07)-Ag(01)-Ag(06)#1	66.29(3)	Ag(01)#1-Ag(03)-Ag(04)	97.56(3)	Cu(0A)-Ag(04)-Ag(02)	57.93(2)
Ag(03)-Ag(02)-Ag(04)	64.06(3)	Ag(02)-Ag(03)-Ag(01)#1	75.99(3)	Cu(0A)-Ag(04)-Ag(03)	73.50(3)
Ag(03)-Ag(02)-Ag(05)	115.91(3)	Ag(02)-Ag(03)-Ag(04)	64.38(3)	Cu(1A)-Ag(04)-Ag(02)	58.69(3)
Ag(03)-Ag(02)-Ag(06)	105.40(3)	Ag(03)-Ag(04)-Ag(02)	51.56(2)	Cu(1A)-Ag(04)-Ag(03)	108.88(3)
Ag(03)-Ag(02)-Ag(07)	79.47(3)	Ag(05)-Ag(04)-Ag(02)	58.69(3)	Cu(1A)-Ag(04)-Cu(0A)	82.04(3)
Ag(03)-Ag(02)-Cu(0A)	79.47(3)	Ag(05)-Ag(04)-Ag(03)	108.88(3)	Ag(02)-Ag(05)-Ag(01)	96.18(3)
Ag(03)-Ag(02)-Cu(1A)	115.91(3)	Ag(05)-Ag(04)-Ag(07)	82.04(3)	Ag(04)-Ag(05)-Ag(01)	70.22(3)
Ag(01)#1-Ag(06)-Ag(02)	69.99(3)	Ag(04)#1-Ag(06)-Ag(01)#1	74.36(3)	Ag(04)-Ag(05)-Ag(02)	67.89(3)
Ag(04)#1-Ag(06)-Ag(02)	117.61(4)	Ag(01)-Ag(07)-Ag(01)#1	180	Ag(01)-Ag(07)-Ag(02)#1	75.00(2)
Ag(01)#1-Ag(07)-Ag(02)	75.00(2)	Ag(01)#1-Ag(07)-Ag(04)	106.38(2)	Ag(04)#1-Ag(07)-Ag(02)	115.38(2)
Ag(01)-Ag(07)-Ag(02)	105.00(2)	Ag(01)-Ag(07)-Ag(04)#1	106.38(2)	Ag(04)-Ag(07)-Ag(02)#1	115.38(2)
Ag(01)#1-Ag(07)-Ag(02)#1	105.00(2)	Ag(01)-Ag(07)-Ag(04)	73.62(2)	Ag(04)-Ag(07)-Ag(02)	64.62(2)
Ag(01)#1-Ag(07)-Ag(04)#1	73.62(2)	Ag(02)#1-Ag(07)-Ag(02)	180	Ag(04)#1-Ag(07)-Ag(02)#1	64.62(2)
Ag(04)-Ag(07)-Ag(04)#1	180	Ag(04)-Ag(07)-Ag(04)#1	180	Cu(0A)-Ag(02)-Ag(04)	57.46(2)
Cu(1A)-Ag(02)-Ag(04)	53.41(2)	Cu(1A)-Ag(02)-Cu(0A)	78.92(3)	N(00J)-Ag(01)-Ag(06)#1	145.0(2)
N(00J)-Ag(01)-Ag(03)#1	106.6(3)	N(00Q)-Ag(04)-C(1)#1	123.7(3)	N(00F)-Ag(06)-Ag(02)	66.3(2)
N(00J)-Ag(01)-C(012)	91.6(3)	N(00J)-Ag(01)-Ag(05)	61.0(2)	N(00J)-Ag(01)-Ag(07)	128.3(2)
N(00J)-Ag(01)-C(013)#1	125.6(4)	N(00D)-Ag(02)-Ag(03)	144.37(19)	N(00D)-Ag(02)-Ag(07)	115.8(2)
N(00J)-Ag(01)-Cu(0A)	128.3(2)	N(00D)-Ag(02)-Ag(04)	151.55(19)	N(00D)-Ag(02)-C(013)	100.6(3)
N(00J)-Ag(01)-C(1)#1	101.9(3)	N(00D)-Ag(02)-Ag(05)	99.0(2)	N(00D)-Ag(02)-Cu(0A)	115.8(2)
N(00P)-Ag(03)-Ag(01)#1	135.1(3)	N(00D)-Ag(02)-Ag(06)	62.6(2)	N(00D)-Ag(02)-Cu(1A)	99.0(2)
N(00P)-Ag(03)-Ag(02)	125.0(3)	N(00Q)-Ag(04)-Ag(02)	109.0(2)	N(00Q)-Ag(04)-Ag(05)	145.6(2)
N(00P)-Ag(03)-Ag(04)	67.0(3)	N(00Q)-Ag(04)-Ag(03)	60.6(2)	N(00Q)-Ag(04)-Ag(06)#1	98.2(2)
N(00Q)-Ag(04)-Ag(07)	120.5(2)	N(00E)-Ag(05)-Ag(01)	65.6(3)	N(00F)-Ag(06)-Ag(04)#1	148.5(2)
N(00Q)-Ag(04)-C(01L)	102.3(4)	N(00E)-Ag(05)-Ag(02)	137.2(3)	C(012)-Ag(01)-Ag(03)#1	71.0(3)
N(00Q)-Ag(04)-Cu(0A)	120.5(2)	N(00E)-Ag(05)-Ag(04)	130.3(2)	C(012)-Ag(01)-Ag(05)	68.6(3)
N(00Q)-Ag(04)-Cu(1A)	145.6(2)	N(00F)-Ag(06)-Ag(01)#1	130.3(2)	C(012)-Ag(01)-Ag(06)#1	107.6(3)
C(012)-Ag(01)-Ag(07)	41.5(3)	C(1)#1-Ag(01)-Ag(07)	90.7(2)	C(013)-Ag(02)-Cu(0A)	88.9(3)
C(012)-Ag(01)-Cu(0A)	41.5(3)	C(1)#1-Ag(01)-C(012)	120.4(4)	C(013)-Ag(02)-Cu(1A)	160.0(2)

C(013)#1-Ag(01)-Ag(03)#1	43.3(2)	C(1)#1-Ag(01)-Cu(0A)	90.7(2)	C(01L)-Ag(02)-Ag(03)	83.8(3)
C(013)#1-Ag(01)-Ag(05)	173.4(3)	C(013)-Ag(02)-Ag(03)	45.4(2)	C(01L)-Ag(02)-Ag(04)	45.1(2)
C(013)#1-Ag(01)-Ag(06)#1	76.3(2)	C(013)-Ag(02)-Ag(04)	106.6(2)	C(01L)-Ag(02)-Ag(05)	42.8(3)
C(013)#1-Ag(01)-Ag(07)	95.4(3)	C(013)-Ag(02)-Ag(05)	160.0(2)	C(01L)-Ag(02)-Ag(06)	155.7(3)
C(013)#1-Ag(01)-C(012)	108.7(4)	C(013)-Ag(02)-Ag(06)	71.8(3)	C(01L)-Ag(02)-Ag(07)	99.9(3)
C(013)#1-Ag(01)-Cu(0A)	95.4(3)	C(013)-Ag(02)-Ag(07)	88.9(3)	C(01L)-Ag(02)-N(00D)	121.5(3)
C(013)#1-Ag(01)-C(1)#1	109.0(4)	C(01L)-Ag(02)-C(013)	126.0(4)	C(013)-Ag(03)-Ag(01)#1	51.3(3)
C(1)#1-Ag(01)-Ag(03)#1	149.1(3)	C(01L)-Ag(02)-Cu(0A)	99.9(3)	C(013)-Ag(03)-Ag(02)	54.7(3)
C(1)#1-Ag(01)-Ag(05)	68.7(3)	C(01L)-Ag(02)-Cu(1A)	42.8(3)	C(013)-Ag(03)-Ag(04)	115.6(3)
C(1)#1-Ag(01)-Ag(06)#1	43.2(2)	C(01L)-Ag(04)-Ag(02)	42.7(3)	C(013)-Ag(03)-N(00P)	173.6(4)
C(01L)-Ag(04)-Ag(03)	73.2(3)	C(1)#1-Ag(04)-Ag(02)	127.0(2)	C(1)#1-Ag(04)-Cu(0A)	87.8(3)
C(01L)-Ag(04)-Ag(05)	45.6(3)	C(1)#1-Ag(04)-Ag(03)	157.9(3)	C(1)#1-Ag(04)-Cu(1A)	79.1(2)
C(01L)-Ag(04)-Ag(06)#1	158.7(3)	C(1)#1-Ag(04)-Ag(05)	79.1(2)	C(01L)-Ag(05)-Ag(01)	120.4(3)
C(01L)-Ag(04)-Ag(07)	98.1(3)	C(1)#1-Ag(04)-Ag(06)#1	46.9(3)	C(01L)-Ag(05)-Ag(02)	47.4(3)
C(01L)-Ag(04)-Cu(0A)	98.1(3)	C(1)#1-Ag(04)-Ag(07)	87.8(3)	C(01L)-Ag(05)-Ag(04)	53.8(3)
C(01L)-Ag(04)-Cu(1A)	45.6(3)	C(1)#1-Ag(04)-C(01L)	122.1(4)	C(01L)-Ag(05)-N(00E)	173.4(4)
C(1)-Ag(06)-Ag(01)#1	52.2(3)	C(012)-Ag(07)-Ag(01)	60.4(3)	C(012)-Ag(07)-Ag(02)#1	105.9(3)
C(1)-Ag(06)-Ag(02)	122.1(3)	C(012)-Ag(07)-Ag(01)#1	119.6(3)	C(012)-Ag(07)-Ag(02)	74.1(3)
C(1)-Ag(06)-Ag(04)#1	52.5(3)	C(012)#1-Ag(07)-Ag(01)	119.6(3)	C(012)#1-Ag(07)-Ag(02)#1	74.1(3)
C(1)-Ag(06)-N(00F)	155.3(4)	C(012)#1-Ag(07)-Ag(01)#1	60.4(3)	C(012)#1-Ag(07)-Ag(02)	105.9(3)
C(012)-Ag(07)-Ag(04)#1	74.8(4)	C(012)#1-Ag(07)-Ag(04)	74.8(4)	C(012)-Ag(07)-Ag(04)	105.2(4)
C(012)#1-Ag(07)-Ag(04)#1	105.2(4)	C(012)-Ag(07)-C(012)#1	180		

Symmetry transformations used to generate equivalent atoms:

#1 -x+1,-y+1,-z+1

Table S9. Selected bond lengths (Å) and bond angles (°) of $Ag_{11.3}Cu_{1.7}$.

Ag(5)-Ag(2)#1	3.3036(9)	Ag(1)-Ag(2)	3.0818(8)	Cu(2)-Cu(1)#1	2.845(6)
Ag(3)-Ag(4)	3.2987(8)	Ag(3)-Cu(2)	3.0762(6)	Ag(3)-Ag(06)#1	2.8369(14)
Ag(1)-Ag(06)	3.2593(15)	Ag(1)-Cu(2)	3.0723(6)	Ag(3)-Ag(2)	2.8306(8)
Ag(1)-Ag(3)	3.2568(8)	Ag(5)-Ag(4)	3.0167(9)	Ag(5)-Cu(2)	2.8162(5)
Ag(06)-Cu(2)	3.2113(15)	Ag(5)-Ag(06)	2.9978(13)	Ag(3)-Cu(1)#1	2.693(7)
Ag(5)-Cu(1)	3.194(6)	Ag(1)-Ag(4)	2.8563(8)	Ag(5)-C(1)	2.515(7)
Ag(1)-Cu(1)	3.106(7)	Cu(2)-Cu(1)	2.845(6)	C(2)-Cu(1)#1	2.485(9)
Ag(5)-C(40)	2.414(9)	Ag(5)-C(32)	2.380(8)	Ag(3)-C(14)	2.332(7)
C(40)-Cu(1)	2.396(14)	Ag(1)-C(32)	2.379(8)	Ag(5)-N(3)#1	2.310(6)
Ag(1)-C(14)	2.294(8)	N(6)-Cu(1)	2.155(9)	Ag(2)-C(14)	2.041(8)
Ag(1)-N(5)	2.281(6)	Ag(06)-N(6)	2.132(6)	Ag(06)-C(40)	2.014(12)
Ag(3)-N(2)	2.266(6)	Ag(4)-N(1)	2.089(7)	Cu(2)-C(1)#1	1.892(8)
Ag(3)-C(40)#1	2.262(8)	Ag(2)-N(4)	2.083(7)	Cu(2)-C(1)	1.892(8)
C(1)-Cu(1)#1	2.208(9)	Ag(4)-C(32)	2.049(8)	Cu(2)-Ag(1)-Ag(2)	80.437(19)
Ag(4)-Ag(5)-Ag(2)#1	137.85(2)	C(32)-Ag(5)-Ag(2)#1	175.2(2)	Cu(2)-Ag(1)-Ag(06)	60.87(3)
Ag(4)-Ag(5)-Cu(1)	103.71(13)	C(32)-Ag(5)-Ag(06)	76.6(2)	Cu(2)-Ag(1)-Cu(1)	54.84(11)
Ag(06)-Ag(5)-Ag(4)	107.21(3)	C(32)-Ag(5)-Cu(2)	95.22(19)	N(5)-Ag(1)-Ag(3)	151.10(15)
Ag(06)-Ag(5)-Ag(2)#1	99.58(3)	C(32)-Ag(5)-C(1)	109.1(3)	N(5)-Ag(1)-Ag(4)	143.95(15)
Cu(2)-Ag(5)-Ag(4)	80.786(18)	C(32)-Ag(5)-C(40)	107.9(3)	N(5)-Ag(1)-Ag(2)	99.19(15)
Cu(2)-Ag(5)-Ag(2)#1	80.554(17)	C(32)-Ag(5)-Cu(1)	79.2(2)	N(5)-Ag(1)-Ag(06)	62.50(16)

Cu(2)-Ag(5)-Ag(06)	66.97(3)	C(40)-Ag(5)-Ag(4)	147.6(3)	N(5)-Ag(1)-Cu(2)	115.45(15)
Cu(2)-Ag(5)-Cu(1)	56.09(9)	C(40)-Ag(5)-Ag(2)#1	70.1(2)	N(5)-Ag(1)-C(14)	120.5(2)
N(3)#1-Ag(5)-Ag(4)	106.38(18)	C(40)-Ag(5)-Ag(06)	42.0(3)	N(5)-Ag(1)-C(32)	100.4(2)
N(3)#1-Ag(5)-Ag(2)#1	60.31(18)	C(40)-Ag(5)-Cu(2)	91.4(2)	N(5)-Ag(1)-Cu(1)	63.82(19)
N(3)#1-Ag(5)-Ag(06)	144.81(17)	C(40)-Ag(5)-C(1)	120.7(3)	C(14)-Ag(1)-Ag(3)	45.72(19)
N(3)#1-Ag(5)-Cu(2)	129.23(16)	C(40)-Ag(5)-Cu(1)	48.1(3)	C(14)-Ag(1)-Ag(4)	85.4(2)
N(3)#1-Ag(5)-C(1)	92.2(2)	Ag(3)-Ag(1)-Ag(06)	118.94(3)	C(14)-Ag(1)-Ag(2)	41.5(2)
N(3)#1-Ag(5)-C(32)	124.5(3)	Ag(4)-Ag(1)-Ag(3)	64.930(19)	C(14)-Ag(1)-Ag(06)	156.37(19)
N(3)#1-Ag(5)-C(40)	102.9(3)	Ag(4)-Ag(1)-Ag(2)	116.14(2)	C(14)-Ag(1)-Cu(2)	101.17(18)
N(3)#1-Ag(5)-Cu(1)	149.9(2)	Ag(4)-Ag(1)-Ag(06)	104.49(3)	C(14)-Ag(1)-C(32)	126.7(3)
C(1)-Ag(5)-Ag(4)	71.94(18)	Ag(4)-Ag(1)-Cu(2)	79.207(19)	C(14)-Ag(1)-Cu(1)	145.7(2)
C(1)-Ag(5)-Ag(2)#1	69.15(18)	Ag(4)-Ag(1)-Cu(1)	109.99(12)	C(32)-Ag(1)-Ag(3)	107.31(18)
C(1)-Ag(5)-Ag(06)	107.83(19)	Ag(2)-Ag(1)-Ag(3)	52.959(18)	C(32)-Ag(1)-Ag(4)	44.94(19)
C(1)-Ag(5)-Cu(2)	41.08(18)	Ag(2)-Ag(1)-Ag(06)	116.26(3)	C(32)-Ag(1)-Ag(2)	160.27(18)
C(1)-Ag(5)-Cu(1)	97.0(2)	Ag(2)-Ag(1)-Cu(1)	105.53(9)	C(32)-Ag(1)-Ag(06)	71.4(2)
C(32)-Ag(5)-Ag(4)	42.62(19)	Cu(2)-Ag(1)-Ag(3)	58.073(15)	C(32)-Ag(1)-Cu(2)	88.89(18)
C(32)-Ag(1)-Cu(1)	81.1(2)	C(40)#1-Ag(3)-Ag(2)	81.9(3)	C(14)-Ag(2)-Ag(1)	48.1(2)
Cu(1)-Ag(1)-Ag(3)	112.10(10)	C(40)#1-Ag(3)-Ag(06)#1	44.8(3)	C(14)-Ag(2)-Ag(3)	54.3(2)
Ag(1)-Ag(3)-Ag(4)	51.656(17)	C(40)#1-Ag(3)-Cu(2)	87.9(3)	C(14)-Ag(2)-N(4)	173.9(3)
Ag(2)-Ag(3)-Ag(1)	60.348(19)	C(40)#1-Ag(3)-N(2)	121.1(3)	Ag(5)-Ag(06)-Ag(1)	70.60(3)
Ag(2)-Ag(3)-Ag(4)	110.43(2)	C(40)#1-Ag(3)-C(14)	124.5(4)	Ag(5)-Ag(06)-Cu(2)	53.81(2)
Ag(2)-Ag(3)-Ag(06)#1	116.39(3)	C(40)#1-Ag(3)-Cu(1)#1	57.0(3)	Ag(3)#1-Ag(06)-Ag(5)	73.30(3)
Ag(2)-Ag(3)-Cu(2)	84.45(2)	Cu(1)#1-Ag(3)-Ag(1)	115.55(13)	Ag(3)#1-Ag(06)-Ag(1)	117.46(5)
Ag(06)#1-Ag(3)-Ag(1)	123.60(4)	Cu(1)#1-Ag(3)-Ag(4)	99.10(11)	Ag(3)#1-Ag(06)-Cu(2)	60.77(3)
Ag(06)#1-Ag(3)-Ag(4)	111.56(4)	Cu(1)#1-Ag(3)-Ag(2)	122.70(14)	Cu(2)-Ag(06)-Ag(1)	56.69(3)
Ag(06)#1-Ag(3)-Cu(2)	65.64(3)	Cu(1)#1-Ag(3)-Cu(2)	58.65(14)	N(6)-Ag(06)-Ag(5)	130.64(18)
Cu(2)-Ag(3)-Ag(1)	57.959(15)	Ag(5)-Ag(4)-Ag(3)	97.67(2)	N(6)-Ag(06)-Ag(1)	66.07(18)
Cu(2)-Ag(3)-Ag(4)	72.705(18)	Ag(1)-Ag(4)-Ag(5)	76.10(2)	N(6)-Ag(06)-Ag(3)#1	149.26(17)
N(2)-Ag(3)-Ag(1)	108.80(17)	Ag(1)-Ag(4)-Ag(3)	63.414(19)	N(6)-Ag(06)-Cu(2)	113.97(18)
N(2)-Ag(3)-Ag(4)	60.60(17)	N(1)-Ag(4)-Ag(5)	135.4(2)	C(40)-Ag(06)-Ag(5)	53.3(3)
N(2)-Ag(3)-Ag(2)	144.52(18)	N(1)-Ag(4)-Ag(1)	123.95(19)	C(40)-Ag(06)-Ag(1)	123.8(3)
N(2)-Ag(3)-Ag(06)#1	97.91(17)	N(1)-Ag(4)-Ag(3)	66.77(18)	C(40)-Ag(06)-Ag(3)#1	52.3(2)
N(2)-Ag(3)-Cu(2)	120.03(18)	C(32)-Ag(4)-Ag(5)	51.9(2)	C(40)-Ag(06)-Cu(2)	88.7(3)
N(2)-Ag(3)-C(14)	101.8(3)	C(32)-Ag(4)-Ag(1)	55.1(2)	C(40)-Ag(06)-N(6)	154.3(3)
N(2)-Ag(3)-Cu(1)#1	92.7(2)	C(32)-Ag(4)-Ag(3)	115.4(2)	Ag(5)#1-Cu(2)-Ag(5)	180
C(14)-Ag(3)-Ag(1)	44.8(2)	C(32)-Ag(4)-N(1)	172.7(3)	Ag(5)-Cu(2)-Ag(1)	75.783(16)
C(14)-Ag(3)-Ag(4)	75.1(2)	Ag(1)-Ag(2)-Ag(5)#1	93.40(2)	Ag(5)#1-Cu(2)-Ag(1)	104.217(16)
C(14)-Ag(3)-Ag(2)	45.3(2)	Ag(3)-Ag(2)-Ag(5)#1	68.75(2)	Ag(5)-Cu(2)-Ag(1)#1	104.217(16)
C(14)-Ag(3)-Ag(06)#1	159.8(2)	Ag(3)-Ag(2)-Ag(1)	66.69(2)	Ag(5)#1-Cu(2)-Ag(1)#1	75.782(16)
C(14)-Ag(3)-Cu(2)	100.2(2)	N(4)-Ag(2)-Ag(5)#1	66.41(19)	Ag(5)#1-Cu(2)-Ag(3)#1	107.624(16)
C(14)-Ag(3)-Cu(1)#1	158.6(2)	N(4)-Ag(2)-Ag(1)	136.1(2)	Ag(5)-Cu(2)-Ag(3)	107.626(16)
C(40)#1-Ag(3)-Ag(1)	129.3(2)	N(4)-Ag(2)-Ag(3)	129.90(18)	Ag(5)#1-Cu(2)-Ag(3)	72.375(16)
C(40)#1-Ag(3)-Ag(4)	155.4(3)	C(14)-Ag(2)-Ag(5)#1	119.3(2)	Ag(5)-Cu(2)-Ag(3)#1	72.375(16)
Ag(5)-Cu(2)-Ag(06)#1	120.78(3)	C(1)#1-Cu(2)-Ag(5)#1	60.9(2)	Ag(3)#1-Cu(1)-Ag(5)	72.04(15)
Ag(5)-Cu(2)-Ag(06)	59.22(3)	C(1)-Cu(2)-Ag(5)#1	119.1(2)	Ag(3)#1-Cu(1)-Ag(1)	128.0(2)
Ag(5)#1-Cu(2)-Ag(06)	120.78(3)	C(1)#1-Cu(2)-Ag(1)#1	107.8(2)	Ag(3)#1-Cu(1)-Cu(2)	67.42(14)
Ag(5)#1-Cu(2)-Ag(06)#1	59.22(3)	C(1)#1-Cu(2)-Ag(1)	72.2(2)	Cu(2)-Cu(1)-Ag(5)	55.23(12)
Ag(5)#1-Cu(2)-Cu(1)#1	68.68(11)	C(1)-Cu(2)-Ag(1)#1	72.2(2)	Cu(2)-Cu(1)-Ag(1)	61.99(14)
Ag(5)-Cu(2)-Cu(1)#1	111.32(11)	C(1)-Cu(2)-Ag(1)	107.8(2)	N(6)-Cu(1)-Ag(5)	120.6(3)
Ag(5)-Cu(2)-Cu(1)	68.68(11)	C(1)#1-Cu(2)-Ag(3)	102.7(2)	N(6)-Cu(1)-Ag(1)	69.2(3)

Ag(5)#1-Cu(2)-Cu(1)	111.32(11)	C(1)#1-Cu(2)-Ag(3)#1	77.3(2)	N(6)-Cu(1)-Ag(3)#1	162.8(4)
Ag(1)-Cu(2)-Ag(1)#1	180	C(1)-Cu(2)-Ag(3)	77.3(2)	N(6)-Cu(1)-Cu(2)	128.7(3)
Ag(1)-Cu(2)-Ag(3)	63.968(14)	C(1)-Cu(2)-Ag(3)#1	102.7(2)	N(6)-Cu(1)-C(1)#1	106.4(4)
Ag(1)#1-Cu(2)-Ag(3)#1	63.968(15)	C(1)#1-Cu(2)-Ag(06)	60.2(2)	N(6)-Cu(1)-C(2)#1	85.4(3)
Ag(1)#1-Cu(2)-Ag(3)	116.033(15)	C(1)-Cu(2)-Ag(06)	119.8(2)	N(6)-Cu(1)-C(40)	125.2(3)
Ag(1)-Cu(2)-Ag(3)#1	116.031(15)	C(1)#1-Cu(2)-Ag(06)#1	119.8(2)	C(1)#1-Cu(1)-Ag(5)	96.6(3)
Ag(1)-Cu(2)-Ag(06)	62.44(2)	C(1)-Cu(2)-Ag(06)#1	60.2(2)	C(1)#1-Cu(1)-Ag(1)	68.4(3)
Ag(1)-Cu(2)-Ag(06)#1	117.55(2)	C(1)#1-Cu(2)-C(1)	180	C(1)#1-Cu(1)-Ag(3)#1	82.1(3)
Ag(1)#1-Cu(2)-Ag(06)	117.56(2)	C(1)-Cu(2)-Cu(1)#1	50.8(2)	C(1)#1-Cu(1)-Cu(2)	41.6(2)
Ag(1)#1-Cu(2)-Ag(06)#1	62.45(2)	C(1)-Cu(2)-Cu(1)	129.2(2)	C(1)#1-Cu(1)-C(2)#1	29.4(3)
Ag(3)#1-Cu(2)-Ag(3)	180	C(1)#1-Cu(2)-Cu(1)#1	129.2(2)	C(1)#1-Cu(1)-C(40)	126.9(4)
Ag(3)#1-Cu(2)-Ag(06)	53.59(2)	C(1)#1-Cu(2)-Cu(1)	50.8(2)	C(2)#1-Cu(1)-Ag(5)	125.6(3)
Ag(3)#1-Cu(2)-Ag(06)#1	126.41(2)	Cu(1)#1-Cu(2)-Ag(1)	116.82(14)	C(2)#1-Cu(1)-Ag(1)	78.4(3)
Ag(3)-Cu(2)-Ag(06)#1	53.59(2)	Cu(1)-Cu(2)-Ag(1)	63.17(14)	C(2)#1-Cu(1)-Ag(3)#1	96.4(2)
Ag(3)-Cu(2)-Ag(06)	126.41(2)	Cu(1)#1-Cu(2)-Ag(3)	53.93(14)	C(2)#1-Cu(1)-Cu(2)	71.0(2)
Ag(06)-Cu(2)-Ag(06)#1	180	Cu(1)-Cu(2)-Ag(3)	126.06(14)	C(40)-Cu(1)-Ag(5)	48.6(2)
C(1)-Cu(2)-Ag(5)	60.9(2)	Cu(1)-Cu(2)-Cu(1)#1	180	C(40)-Cu(1)-Ag(1)	116.4(3)
C(1)#1-Cu(2)-Ag(5)	119.1(2)	Ag(1)-Cu(1)-Ag(5)	70.19(14)	C(40)-Cu(1)-Ag(3)#1	52.4(2)
C(40)-Cu(1)-Cu(2)	91.0(3)	C(40)-Cu(1)-C(2)#1	148.6(4)		

Symmetry transformations used to generate equivalent atoms:

#1 -x+1,-y+1,-z+1

References

1 G. M. Sheldrick, *Acta Crystallogr., Sect. C: Struct. Chem.*, 2015, **A71**, 3–8.
2 O. V. Dolomanov, L. J. Bourhis, R. J. Gildea, J. A. K. Howard and H. Puschmann, *J. Appl. Cryst.*, 2009, **42**, 339–341.
3 G. M. Sheldrick, *Acta Crystallogr., Sect. C: Struct. Chem.*, 2015, **C71**, 3–8.
4 H. V. R. Dias, S. A. Polach and Z. Wang, *J. Fluor. Chem.*, 2000, **103**, 163–169.
5 (a) F. Neese, *Wiley Interdiscip. Rev.: Comput. Mol. Sci.*, 2011, **2**, 73–78; (b) F. Neese, *Wiley Interdiscip. Rev.: Comput. Mol. Sci.*, 2017, **8**, e1327.
6 (a) J. P. Perdew, K. Burke and M. Ernzerhof, *Phys. Rev. Lett.*, 1996, **77**, 3865–3868; (b) J. P. Perdew, K. Burke and M. Ernzerhof, *Phys. Rev. Lett.*, 1997, **78**, 1396–1396.
7 F. Weigend and R. Ahlrichs, *Phys. Chem. Chem. Phys.*, 2005, **7**, 3297–3305.
8 D. Andrae, U. Häußermann, M. Dolg, H. Stoll and H. Preuß, *Theor. Chim. Acta*, 1990, **77**, 123–141.
9 F. Weigend, *Phys. Chem. Chem. Phys.*, 2006, **8**, 1057–1065.
10 T. Lu and F. Chen, *J. Comput. Chem.*, 2011, **33**, 580–592.
11 W. Humphrey, A. Dalke and K. Schulten, *J. Mol. Graphics*, 1996, **14**, 33–38.
12 (a) AMS 2018, 2018. SCM, Theoretical Chemistry, *Vrije Universiteit*, Amsterdam, The Netherlands, http://www.scm.com/; (b) C. F. Guerra, J. G. Snijders, G. te Velde and E. J. Baerends, *Theor. Chem. Acc.* 1998, **99**, 391−403; (c) G. te Velde, F. M. Bickelhaupt, E. J. Baerends, C. F. Guerra, S. J. A. Van Gisbergen, J. G. Snijders and T. Ziegler, *J. Comput. Chem.* 2001, **22**, 931−967.
13 E. van Lenthe and E. J. Baerends, *J. Comput. Chem.*, 2003, **24**, 1142–1156.
14 (a) E. van Lenthe, E. J. Baerends and J. G. Snijders, *J. Chem. Phys.*, 1994, **101**, 9783–9792; (b) E. van Lenthe, E. J. Baerends and J. G. Snijders, *J. Chem. Phys.*, 1993, **99**, 4597–4610; (c) E. van Lenthe, J. G. Snijders and E. J. Baerends, *J. Chem. Phys.*, 1996, **105**, 6505–6516.
15 R. Rüger, E. van Lenthe, T. Heine and L. Visscher, *J. Chem. Phys.*, 2016, **144**, 184103–13.
16 H. Kudo, R. Hayashi, K. Mitani, T. Yokozawa, N. C. Kasuga and T. Nishikubo, *Angew. Chem., Int. Ed.*, 2006, **45**, 7948–7952.
17 M. J. Turner, J. J. McKinnon, S. K. Wolff, D. J. Grimwood, P. R. Spackman, D. Jayatilaka and M. A. Spackman, 2017. University of Western Australia. http://hirshfeldsurface.net.